

# Design of interdigitated transducers for acoustofluidic applications

Cite as: Nano. Prec. Eng. 5, 035001 (2022); doi: 10.1063/10.0013405

Submitted: 30 April 2022 • Accepted: 23 July 2022 •

Published Online: 25 August 2022



View Online



Export Citation



CrossMark

Shuren Song,<sup>a)</sup> Qi Wang,<sup>a)</sup> Jia Zhou,<sup>a)</sup> and Antoine Riaud<sup>a)</sup>

## AFFILIATIONS

State Key Laboratory of ASIC and System, School of Microelectronics, Fudan University, Shanghai, People's Republic of China

<sup>a)</sup>Authors to whom correspondence should be addressed: [jia.zhou@fudan.edu.cn](mailto:jia.zhou@fudan.edu.cn) and [antoine\\_riaud@fudan.edu.cn](mailto:antoine_riaud@fudan.edu.cn)

## ABSTRACT

Interdigitated transducers (IDTs) were originally designed as delay lines for radars. Half a century later, they have found new life as actuators for microfluidic systems. By generating strong acoustic fields, they trigger nonlinear effects that enable pumping and mixing of fluids, and moving particles without contact. However, the transition from signal processing to actuators comes with a range of challenges concerning power density and spatial resolution that have spurred exciting developments in solid-state acoustics and especially in IDT design. Assuming some familiarity with acoustofluidics, this paper aims to provide a tutorial for IDT design and characterization for the purpose of acoustofluidic actuation. It is targeted at a diverse audience of researchers in various fields, including fluid mechanics, acoustics, and microelectronics.

© 2022 Author(s). All article content, except where otherwise noted, is licensed under a Creative Commons Attribution (CC BY) license (<http://creativecommons.org/licenses/by/4.0/>). <https://doi.org/10.1063/10.0013405>

## KEYWORDS

Acoustic field, Surface acoustic wave, Transducer, Finite-element analysis, Simulation, Acoustical properties, Lab-on-a-chip, Acoustic wave attenuation

## I. AIM AND SCOPE

Since their initial realization by White and Volmer in 1965,<sup>1</sup> interdigitated transducers (IDTs) have been widely used, first in radar and then in telecommunications at the dawn of the mobile-phone era, and they have recently been repurposed for a wide range of applications,<sup>2</sup> one of the most spectacular being the ultrasonic manipulation of fluids with surgical precision.<sup>3</sup> In this emerging field, nonlinear acoustic phenomena such as acoustic radiation pressure and acoustic streaming are used to mix microliter droplets, pump liquids through nanoscale channels, sort biological cells, and capture and move particles without contact. The field has been extensively reviewed over the past decade, and a number of excellent papers provide an overview of design of applications of acoustofluidics, including the tutorial series in *Lab on a Chip*,<sup>4</sup> a tutorial on the efficiency of acoustofluidic actuation using IDTs,<sup>5</sup> reviews of the field as a whole,<sup>6</sup> reviews of nanoscale-acoustofluidics,<sup>7</sup> material synthesis,<sup>8</sup> acoustofluidic chips that can be reconfigured over time,<sup>9</sup> unconventional acoustofluidics,<sup>10</sup> bioapplications,<sup>11,12</sup> acoustic tweezers,<sup>13</sup> and so on. IDTs are just one particular way to generate acoustic waves in fluids, and other popular tools include transducer networks,<sup>14,15</sup> thin-film transducers,<sup>16</sup> resonant cavities,<sup>17</sup> and

phononic crystals.<sup>18,19</sup> Compared with these methods, however, the use of IDTs simplifies miniaturization and mass production, allows the use of higher frequencies, and provides control over the spatial distribution of the acoustic field. Despite their considerable importance in the field, the design of IDTs for acoustofluidic devices has not been reviewed yet.

Differing from the original design considerations of IDTs (such as bandwidth and energetic efficiency), acoustofluidic applications are mainly concerned with (i) the ultrasonic power and (ii) the spatial distribution of the acoustic field. The power requirement stems from the nonlinear nature of the acoustic phenomena used in acoustofluidic chips: for instance, high power levels are needed to counteract surface tension phenomena when splitting droplets or ejecting their content into the air. The spatial control of the acoustic field is important to precisely manipulate micro-objects, such as in fluorescence-activated ultrasonic cell sorting or selective acoustic tweezers. The considerable progress that has been made in enhancing ultrasonic power and refining the spatial distribution of the generated acoustic field has not been covered by the otherwise high-quality monographs on surface acoustic wave (SAW) filter design.<sup>20–22</sup>

This review focuses on the generation of powerful and spatially controlled acoustic fields for applications to acoustofluidic devices. We begin with a tutorial reviewing some fundamentals about electroacoustic transducers, acoustic waves in solids and fluids, and IDTs that were developed up to the 1990s. We then review how the transition to acoustofluidic applications marked a big change in emphasis from the subwavelength structure of the IDT (which determines the bandwidth and energetic efficiency of the transducer) to its superstructure over many wavelengths. Optimizing the IDT superstructure addresses the challenges of acoustofluidics by enabling the generation of more powerful focused acoustic waves and fine control over the spatial distribution of the acoustic field. Finally, we review several experimental methods for the characterization of the synthesized acoustic fields, on the solid and in the fluid.

## II. ELECTROACOUSTIC TRANSDUCTION

Interdigitated transducers are interlocked electrodes deposited on a piezoelectric crystal. To optimize the transducer power, it is helpful to consider a simpler model of a flat longitudinal wave transducer.

### A. Piezoelectric effect

In nonpiezoelectric materials, a mechanical displacement  $u$  induces a stress  $T = c\partial_z u$ , where  $c$  is the stiffness of the material. In addition, an electrical displacement  $D$  induces an electric field  $E = D/\epsilon$ , with  $\epsilon$  the electric permittivity of the material. When the material is an insulator (like most piezoelectric materials) and electro-neutral, the electric current is related to the electric displacement  $\partial_t D = I(t)/A$ , with  $A$  the cross-section of the transducer.

In piezoelectric materials, the electrical and mechanical fields are entangled by the piezoelectric coupling coefficient  $e$ . The stress now reads  $T = c^D \partial_z u - (e/\epsilon)D$ , where  $c^D$  is the stiffness at constant electric displacement,  $c^D = c^E + e^2/\epsilon$ , with  $c^E$  the stiffness at constant electric field, which has been extensively tabulated.

Deriving the stress over time and substituting the electric displacement, we get<sup>22</sup>

$$\partial_t T = c^D \partial_z v - \frac{e}{A\epsilon} I(t). \quad (1)$$

This equation couples (i) the stress in the material, (ii) the mechanical vibration of the material, and (iii) the electric current applied across it. Using Newton's law  $\rho\partial_t v = -\partial_z T$ , we get the equation of a plane longitudinal electroacoustic wave propagating through a piezoelectric material:<sup>22</sup>

$$\rho\partial_t^2 v = c^D \partial_z^2 v. \quad (2)$$

We next consider the electrical characteristics of a transducer made of this piezoelectric material.

### B. Equivalent circuit of a bulk transducer

Considering a slab of thickness  $d$  of the material described by Eq. (2), the general solution for the electroacoustic field in the material is a combination of a forward-propagating acoustic wave of amplitude  $a$  and a backward-propagating wave of amplitude  $b$ , such

that the total velocity field reads  $v = ae^{-ikz} + be^{ikz}$ , where  $k = \omega/V$  is the acoustic wavenumber in the piezoelectric material at angular frequency  $\omega$ , with  $V = \sqrt{c^D/\rho}$  the acoustic wave velocity in the piezoelectric.

We now assume that the slab is exposed to a current  $I$  and irradiated by an incident field from the left  $v_1 = v(z = -d)$  and an incident field from the right  $v_2 = -v(z = 0)$ , and seek an expression for the voltage  $U$  across the slab, together with the resulting pressures  $p_1$  and  $p_2$  on each side. We get the impedance matrix of the transducer that connects stresses (force and voltage) on each side of the transducer to fluxes (vibration field and current):<sup>22</sup>

$$\begin{bmatrix} p_1 \\ p_2 \\ U \end{bmatrix} = -i \begin{bmatrix} Z/\tan(kd) & Z/\sin(kd) & e/(A\epsilon\omega) \\ Z/\sin(kd) & Z/\tan(kd) & e/(A\epsilon\omega) \\ e/(A\epsilon\omega) & e/(A\epsilon\omega) & 1/\omega C_0 \end{bmatrix} \begin{bmatrix} v_1 \\ v_2 \\ I \end{bmatrix}, \quad (3)$$

where  $Z = \rho V = \sqrt{\rho c^D}$  is the acoustic impedance of the material and  $C_0 = \epsilon A/d$  is the static capacitance of the transducer.

Such a transducer admits an equivalent circuit as shown in Fig. 1(b). If the transducer operates at sufficiently low frequency (<100 MHz) that the loading of the electrodes can be neglected, the values of the components at the resonance frequency  $f = f_p = V/(2d)$  read:<sup>22</sup>

$$C_0 = \epsilon A/d, \quad (4)$$

$$X_a = 0, \quad (5)$$

$$R_a = \frac{4K^2}{\pi C_0 \omega_p} \frac{Z}{Z_1 + Z_2}. \quad (6)$$

The matching impedance  $L_s$  is chosen to optimize the transducer power, as explained hereinafter.

We deduce that the emitted power from the transducer is

$$\langle \mathcal{P} \rangle = \frac{1}{2} \frac{R_a U_0^2}{(R_0 + R_a)^2 + [1/(C_0 \omega_p) - L_s \omega_p]^2}. \quad (7)$$

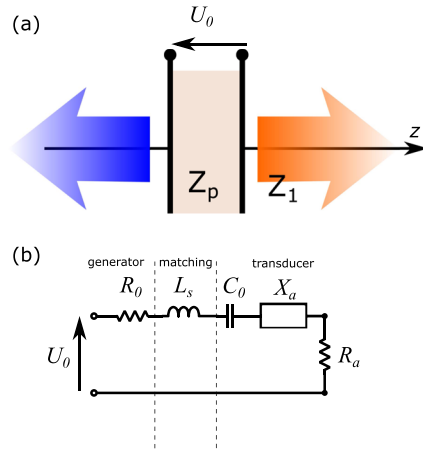


**FIG. 1.** Equivalent circuit of piezoelectric transducer. (a) When exposed to a voltage  $U_0$ , the transducer emits waves in two opposite directions. (b) Equivalent electric circuit. The impedance  $X_a$  is zero at resonance.

Therefore, the emitted power is maximized when the matching impedance exactly cancels the capacitance of the transducer, that is,  $L_s = 1/(C_0 \omega_p)^2$ . Upon matching, Eq. (7) indicates that the emitted power ( $\langle P \rangle$ ) is maximum for  $R_0 = R_a$ . Most signal generators use  $R_0 = 50 \Omega$ , and therefore transducers should be designed to match  $R_a = 50 \Omega$  whenever possible.

### C. Radiofrequency electronics

Electrically mismatched transducers not only work less efficiently, but are also less reliable and may even damage the electrical source to which they are connected.<sup>23</sup> These issues can be avoided with some elementary considerations.

#### 1. Reliability of transducers connected to long cables

When operating at low frequency, the transducer impedance is relatively easy to match. However, when a transducer is connected to a cable or a PCB track, the input impedance of the assembly may differ significantly from that of the transducer itself. This happens when the electromagnetic wavelength  $\lambda_{EM}$  of the electric excitation signal is comparable to the cable length, which is the hallmark of radiofrequency electronics. The wavelength reads  $\lambda_{EM} = V_{EM}/f$ , where the electromagnetic wave speed in cables is given by  $V_{EM} = \chi V_{EM,0}$ , with  $\chi \lesssim 1$  the velocity factor of the cable. For instance, a 30 MHz signal in a typical RG-213 coaxial cable ( $\chi = 0.66$ ) has a wavelength of 6.6 m. Therefore, any cable longer than 1 m may induce significant changes in the input impedance of the cable and transducer assembly. This problem can be minimized by matching the transducer impedance to that of the impedance line. In practice, the transducer is soldered to a short coaxial cable, and the input impedance of this small assembly is measured and matched to  $50 \Omega$  with an electric circuit implemented directly at the end of the PCB cable. Such circuits can be automatically designed using T-shaped or II-shaped architecture calculators available online (see Fig. 2).

#### 2. Voltage standing wave ratio, reflected power, and danger to radiofrequency power supplies

The electric signal sent from the power source to the transducer is a solution of the D'Alembert equation and can therefore be written as two counter-propagating electric potentials. The forward wave  $\phi_I$  transmits the power from the power source to the transducer, whereas the reflected wave  $\phi_R$  is due to a mismatch between the

transducer and the transmission line. The amplitude of the reflected wave is given by  $\phi_R = \Gamma \phi_I$ :

$$\Gamma = \frac{Z_e - Z_{\text{line}}}{Z_e + Z_{\text{line}}}, \quad (8)$$

which vanishes when  $Z_e = Z_{\text{line}}$ .

The superposition between incident and reflected electromagnetic waves results in a standing wave pattern with a ratio between the maximum and the minimum amplitude given by the voltage standing wave ratio (VSWR):

$$\text{VSWR} = \frac{|\phi_I| + |\phi_R|}{|\phi_I| - |\phi_R|} = \frac{1 + |\Gamma|}{1 - |\Gamma|}. \quad (9)$$

Amplifiers are designed to accept a certain current at their output, which may be exceeded if the VSWR is too large for too long. Besides being due to a mismatched transducer, this may also happen if the generator is turned on when the transducer is not connected (open-circuit) or shorted for some reason (malfunctioning transducer).

While these concepts have been introduced using the example of a one-dimensional transducer, they are equally relevant for the interdigitated transducers presented in this review.

## III. ACOUSTIC WAVES IN SOLIDS AND FLUIDS

The power dissipated by the IDTs is used to generate acoustic waves (Table I). There is a considerable variety of waves that can be generated by IDTs, some of them useful for actuation and others more suitable for sensing. Some of these waves have very stringent existence conditions, whereas others are almost always present.

In this section, we present the main kinds of acoustic waves. When applied to piezoelectric materials, all these waves are coupled to an electric potential that can be used not only for generation and detection, but also for particle manipulation using the electrophoresis effect (Fig. 3).<sup>24–26</sup>

### A. Acoustic waves in solids

This section first presents the waves that exist only in solids (without any fluid loading). They are valuable for conveying acoustic energy from the IDT to a nearby liquid.

### B. Bulk waves

Bulk waves exist in all solids, and all the waves that will be considered subsequently are linear combinations of bulk waves. They are therefore very instructive for any IDT design.

In isotropic materials, two types of waves are possible: longitudinal waves with polarization directed along the propagation direction  $\mathbf{n}$  and shear waves with polarizations directed normal to the propagation direction  $\mathbf{n}$ . In anisotropic solids, the waves also feature three modes, but they have mixed components: the pseudo-longitudinal mode includes some transverse displacement, and conversely the pseudo-transverse modes include some longitudinal displacement.

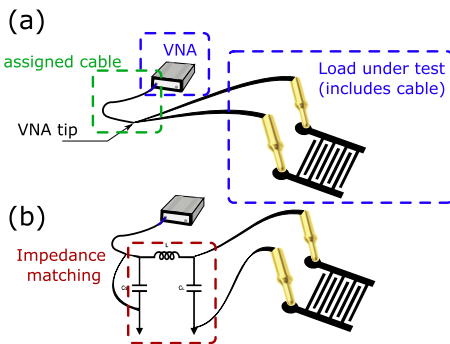


**FIG. 2.** Steps to match a circuit with a VNA: (a) measuring the impedance; (b) implementing a Pi-shaped impedance matching circuit at the measurement spot.

**TABLE I.** Comparison of the various types of sound waves, including conditions of generation, propagation direction, and application scenarios.  $h$  and  $p$  denote the substrate thickness and electrode period (from positive to positive electrode), respectively. TV and TH are abbreviations for transverse vertical and transverse horizontal displacements.

Type of sound wave	Conditions of generation	Propagation direction	Application scenario
Bulk wave	$p > \lambda_{\text{bulk}}$	Set by the dispersion relation $k_x^2 + k_z^2 = \left(\frac{\omega}{c_{\text{bulk}}}\right)^2$	Protect the IDT (IDT on one side of the substrate and microfluidic chip on the other)
Surface-skimming bulk wave	$p = \lambda_{\text{bulk}}$	Along the surface but with leaks towards the bulk	High power
Rayleigh	$p = \lambda_{\text{SAW}}$	Along the surface	Transmit acoustic power over many wavelengths from IDT (dry) to the liquid
Lamb	$h < \lambda_{\text{SAW}}$	Along the surface	Transmit acoustic power over many wavelengths from IDT (dry) to the liquid, protect the IDT (Hydra)
Sezawa	Need coating softer than bulk	Along the surface	Transmit acoustic power over many wavelengths from IDT (dry) to the liquid (when using piezoelectric coatings like ZnO or AlN)
Love	Need coating softer than bulk	Along the surface	Transmit acoustic signal over many wavelengths from IDT (dry) to the liquid, for sensing
Bleustein–Gulyaev	Need piezoelectric coupling	Along the surface but with deep penetration in the bulk	Transmit acoustic signal over many wavelengths from IDT (dry) to the liquid, used for dielectrophoresis
Leaky SAW	Need liquid loading	Along the surface	Sharp attenuation allows sensing density, sound velocity of liquid
Radiation of a bulk wave	Need TV component and liquid loading	Inside the liquid, with the Rayleigh angle set by the dispersion relation $k_{\text{SAW}}^2 + k_z^2 = \left(\frac{\omega}{c_{\text{SAW}}}\right)^2$	Transmit acoustic power from solid to liquid, acoustic mixing, pumping, manipulation, trapping...
Radiation of a viscoacoustic wave	Need TH component and liquid loading	Not propagative	Not applied yet, Rayleigh streaming over large distances
Scholte wave	Contact line	Along the surface	Transmit acoustic power over many wavelengths next to the liquid surface, used for acoustic manipulation
Evanescence wave	Small scattering obstacles	Not propagative	Acoustic trapping

The dispersion relation of these waves in a piezoelectric solid is obtained by solving the secular equation:<sup>22</sup>

$$\left( \rho V^2 \delta_{il} - \Gamma_{il} + \frac{\gamma_i \gamma_l}{\epsilon} \right) u_l^{(0)} = 0, \quad (10)$$

where  $\rho$  is the material density,  $V$  is the unknown sound speed,  $\Gamma_{il} = c_{ijkl}^E n_j n_k$  is the Christoffel tensor ( $c^E$  is the stiffness tensor at constant electric field), and  $\gamma_i = e_{kij} n_j n_k$  is the piezoelectric coupling coefficient. The vibration components  $u_l^{(0)}$  are considered in an abstract way and include the electric potential moving with the wave. This equation admits nontrivial solutions only if  $\det(\rho V^2 \delta_{il} - \Gamma_{il} + \gamma_i \gamma_l / \epsilon) = 0$ , which yields a polynomial in  $V^2$  with three real roots that correspond to the sound speeds of the pseudo-longitudinal and pseudo-transverse waves. The different components  $u_l^{(0)}$  can then be deduced by setting one of them (often the electric potential) to unity. We note that setting the electric potential to unity

in Eq. (10) can recast the propagation problem as an eigenvalue problem and directly yield the sound speed and the vibration components in one step. In Eq. (10), the velocity  $V$  is increased by the piezoelectric coupling  $\gamma_i \gamma_l / \epsilon$ . This piezoelectric stiffening provides an excellent indication of the electromechanical coupling  $K^2$ . When the coupling is small,  $K^2$  is proportional to the difference in sound speed  $\Delta V$  between the case where piezoelectric stiffening is included and the same material where the stiffening is omitted:  $K^2 \simeq 2 \frac{\Delta V}{V}$ . This allows rapid analysis of many materials and propagation directions simply by solving as many independent eigenvalue problems.

Bulk waves also offer a glimpse of some peculiar phenomena found in anisotropic materials:<sup>29</sup>

- beam stirring: the wave phase does not propagate in the same direction as the wave energy (i.e., phase speed and group speed are not collinear);

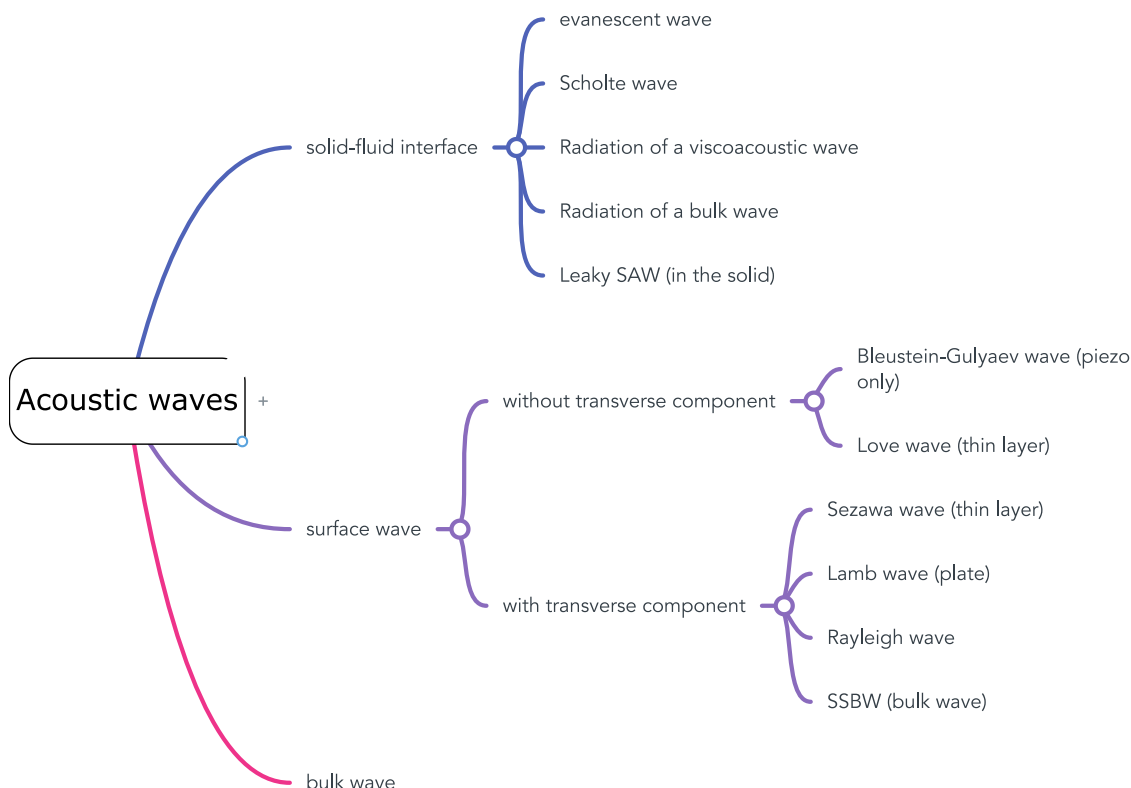


FIG. 3. The most common types of acoustic waves that can be excited using an IDT.

- self-focusing: this is observed when the wave slowness ( $1/V$ ) features some inflection points. The wave spontaneously forms caustics in some directions.

### C. Surface acoustic waves

Unlike bulk waves, SAWs are guided waves and propagate along a surface. Their attenuation from a point source scales as  $1/\sqrt{r}$ , and they nearly do not attenuate when they are generated from a line source such as an IDT, which makes them especially attractive for conveying information or power. However, they have much more stringent generation conditions than bulk waves.

#### 1. Transverse vertical waves

Transverse vertical waves can transmit energy to the fluid located over them. Thus, they are highly suitable for building actuators.

*a. Rayleigh waves.* Rayleigh waves [see Fig. 4(a)] were historically the first surface waves to be described rigorously.<sup>30</sup> Isotropic solids can transmit pure Rayleigh waves, which combine a longitudinal and transverse vertical displacement into an elliptical motion.

The energy of pure Rayleigh waves is confined within approximately one wavelength of the surface. In anisotropic solids, Rayleigh waves keep a strong transverse vertical component but couple it

with a transverse horizontal component. In addition, Rayleigh waves on piezoelectric solids are also coupled to an electric potential. In some instances, they may also attenuate over a much larger depth or completely lose their transverse vertical component (see the Bleustein–Gulyaev waves).

Rayleigh waves are nondispersive, and their velocity is slightly lower than that of transverse vertical bulk waves. The exact calculation of Rayleigh wave propagation involves solving an algebraic–differential equation that combines the dispersion relation of bulk plane waves in solids with a stress-free boundary condition at the surface (top) of the solid and an infinite half-space toward the bottom.<sup>31</sup>

A large number of piezoelectric materials can be used to generate Rayleigh waves, including gallium arsenide (GaAs), cadmium sulfide (CdS), zinc oxide (ZnO), lithium tetraborate ( $\text{Li}_2\text{B}_4\text{O}_7$ ), langasite ( $\text{La}_3\text{Ga}_5\text{SiO}_{12}$ ), quartz, lithium tantalate ( $\text{LiTaO}_3$ ), and lithium niobate ( $\text{LiNbO}_3$ ).<sup>7,32</sup> The electromechanical coupling coefficient  $K_R^2$  is a good indicator of piezoelectric material performance. Because SAW coupling is generally limited, the coupling coefficient is approximated well by  $K_R^2 \approx 2\Delta V/V = 2(V_R - V_{\text{short}})/V_R$ . Here,  $V_R$  and  $V_{\text{short}}$  are the wave velocities for two electrical boundary conditions on the top surface: (i) open-circuit (no electrode) and (ii) short circuit, respectively. Table II lists some of the most common cuts of  $\text{LiNbO}_3$ , together with their electromechanical coupling coefficients and velocities.<sup>33–37</sup> The Y-152 cut proposed by Zhang *et al.*<sup>38</sup>

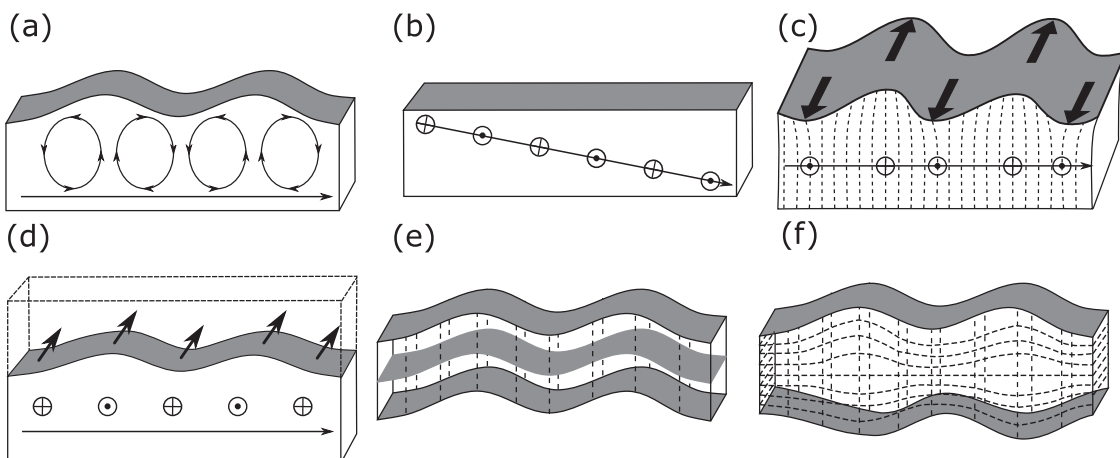


**FIG. 4.** Various types of SAWs:<sup>27</sup> (a) pure Rayleigh wave; (b) Surface-skimming bulk wave;<sup>28</sup> (c) Love wave; (d) leaky SAW; (e) antisymmetric and (f) symmetric Lamb waves propagating in a plate. Solid motion is represented by the ellipses and  $\oplus$  and  $\ominus$  symbols, while energy propagation is shown by the arrows.

**TABLE II.** Electromechanical coupling coefficients and velocity of commonly used piezoelectric materials.<sup>33–38</sup>

Cut	$K_R^2$	Velocity $V$ ( $\text{m s}^{-1}$ )
YZ	4.82	3488
ZX	0.53	3798
ZY	2.25	3903
XY	3.58	3748
$20^\circ$ XY	1.6	3727
$120^\circ$ XY	4.1	3403
XZ	5	3483
YX	1.54	3769
$36^\circ$ YX	16.7	4802
$41^\circ$ YX	17.2	4752
$64^\circ$ YX	10.8	4692
$128^\circ$ YX	5.3	3992
$152^\circ$ Y	$4 \pm 1.5$	$3700 \pm 200$

has been specially designed to reduce anisotropy with acoustofluidic applications in mind.

Rayleigh waves are strongly anisotropic. As a result, transducer design for complex fields must take anisotropy into account. Examples of complex Rayleigh waves include focused waves<sup>39</sup> and swirling SAWs,<sup>40</sup> which are a two-dimensional analog of acoustic vortices generalized to anisotropic media.

*b. Lamb waves.* When the solid body carrying the surface wave is too thin to encompass the full Rayleigh wave (if the solid is thinner than one acoustic wavelength in the case of isotropic solids), the surface wave should be described as a Rayleigh–Lamb wave.

In the extreme case where the plate is much thinner than the acoustic wavelength, the surface wave is called a Lamb wave, which can be symmetric or antisymmetric.<sup>41</sup> Lamb waves feature a number of modes, are dispersive, and propagate much more slowly

than Rayleigh waves. In the case of a piezoelectric, the displacement achieved with Lamb waves (and even Rayleigh–Lamb waves<sup>42</sup>) is much larger than that with Rayleigh waves. It is therefore not surprising that these waves were among the first to be used in acoustofluidic applications.<sup>43</sup> The experiments of Rezik *et al.*<sup>42</sup> illustrate well the different propagation modes of Rayleigh and Lamb waves. Lamb waves make both sides of the plate vibrate, which allows the IDT to be placed on the opposite side of the liquid sample to protect it from the environment.<sup>44</sup> Interestingly, the velocity of Lamb waves is nearly isotropic, even for anisotropic substrates. This allows the synthesis of isotropic acoustic fields using anisotropic substrates.<sup>45,46</sup>

*c. Sezawa waves.* Sezawa waves (second Rayleigh mode) appear on hard materials coated with a softer layer when the layer thickness is a significant fraction of the wavelength.<sup>47,48</sup> Sezawa waves are most often seen when working with piezoelectric coatings such as AlN or ZnO. Sezawa waves feature a high velocity, high electromechanical coupling, and a transverse vertical displacement.<sup>49,50</sup> These three characteristics make them well suited not only for droplet mixing<sup>51</sup> but also for droplet jetting and nebulization<sup>52–54</sup> despite the lower intrinsic coupling of AlN and ZnO compared with bulk crystals such as LiNbO<sub>3</sub>. Sezawa waves are dispersive.

*d. Surface-skimming bulk waves.* When an IDT is driven at an excessive frequency, it tends to generate bulk waves. Bulk waves are usually a nuisance, since they can reflect from the back of the substrate and come back to the top, which results in spurious acoustic spots.

Surface-skimming bulk waves (SSBWs) are bulk waves that propagate horizontally, which makes them similar to SAWs (and therefore they have been classified as SAWs in this review). They feature a shear displacement component and propagate just below the surface of a piezoelectric substrate.<sup>28,55</sup> Owing to their bulk-wave nature, SSBWs generated from a point decay as  $1/r$ , where  $r$  is the distance to the source, and those from a line source (such as a finger pair of an IDT) radiate to the bottom of the substrate and

decay as  $1/\sqrt{r}$ . They feature a much higher piezoelectric coupling than Rayleigh waves and can therefore be useful for short-range actuation. Nevertheless, one should be wary of reflections at the bottom of the substrate, although some clever designs use this for multiplex droplet actuation.<sup>56</sup> SSBWs also allow the IDT to be protected from the fluid by placing it on the opposite side of the solid.<sup>45</sup>

## 2. Transverse horizontal waves

Transverse horizontal waves do not transmit energy to the fluid located over them and therefore experience little attenuation when propagating under a fluid. Yet, they propagate more slowly when the substrate is loaded with a fluid, and they can attenuate owing to the generation of shear waves in the viscoacoustic boundary layer, which makes them sensitive to fluid density and viscosity. Therefore, they are mostly used to build sensors.<sup>2,49</sup> They can also be used to generate Rayleigh acoustic streaming without inducing acoustic radiation pressure or Eckart streaming.

*a. Love waves.* Love waves were discovered soon after Rayleigh waves. They combine a transverse-horizontal (TH) motion with longitudinal component. Unlike Rayleigh waves, they do not exist in homogeneous solids and can only propagate at the interface between a material and a softer layer with a slower transverse wave velocity [see Fig. 4(c)].<sup>57,58</sup> Love-mode acoustic devices are very well suited for the construction of biosensors in gaseous and liquid environments, because their low attenuation enables the use of very high frequencies and provides a fine measurement of the wave velocity, which allows the detection of very small amounts of added mass.<sup>59–61</sup> Similar to a Rayleigh wave, a Love wave penetrates by approximately one wavelength into the lower layer. If the upper soft layer is much thinner than the acoustic wavelength, most of the wave energy will be confined to the lower layer. However, at high frequency (thick soft layer), the Love wave will be confined at the interface between the two solids and become a Stoneley wave. Similarly to Lamb and Sezawa waves, Love waves are dispersive.

*b. Bleustein–Gulyaev waves.* Bleustein–Gulyaev (BG) waves are shear-horizontal surface waves that propagate on piezoelectric materials.<sup>62,63</sup> These waves were independently predicted by Bleustein and Gulyaev. They can propagate in piezoelectric materials, but find no elastic counterparts in purely elastic homogeneous materials.<sup>64,65</sup> Unlike Rayleigh waves, BG waves penetrate much deeper in the solid (10–100 wavelengths). Therefore, these waves are very insensitive to the composition of any coating or fluid that would be placed on the propagation medium. Owing to the piezoelectric effect, BG waves have been used to induce electrophoresis without the influence of radiation pressure and Eckart acoustic streaming (although Rayleigh streaming continues to disturb the experiment).<sup>26</sup>

## D. Acoustic waves at the interface between solids and fluids

When a fluid is placed on the path of an SAW, the wave energy is partially transmitted to the fluid. Some waves transfer their energy

completely to the fluid within a few wavelengths, whereas others can travel long distances with little attenuation. Some waves will only trigger an evanescent wave in the fluid, but others will create a traveling pressure wave. This subsection analyses in detail the conditions associated with each phenomenon.

### 1. Radiation of a bulk wave by a Rayleigh wave propagating under a liquid

In most solids, the SAW velocity  $V_R$  is larger than the sound velocity in the fluid  $V_F$ . When such a wave encounters a fluid, it forms a supersonic cone and radiates into the fluid with a Rayleigh angle  $\sin \theta_R = V_F/V_R$ , with  $V_F$  the sound velocity in the fluid (this is analogous to the Cherenkov effect). This radiation splits the channel into a silent edge and an irradiated volume. This has long been seen as detrimental to acoustofluidic applications, which usually assume that the channel is uniformly exposed to acoustic waves. Recently, Collins *et al.*<sup>66</sup> have challenged this view and instead have elegantly shown that the phenomenon allows the construction of complex acoustic fields with the simplest transducers by using the channel walls as boundary conditions. This shifts the hurdle of designing complex anisotropic transducers to one of designing complex diffractive elements accounting for the three-dimensional isotropic wave propagation in fluids, which can be done by a range of methods<sup>67,68</sup> (see Sec. V B).

When the solid is anisotropic (e.g., when using  $\text{LiNbO}_3$ ), the SAW velocity  $V_R$  depends on the propagation direction  $\psi$ . This also means that the Rayleigh angle depends on the propagation direction, which induces a degeneracy of the radiated waves as they travel away from the surface. The degeneracy is a linear process, and therefore the SAW field on the surface can be predistorted to obtain a desired field at an arbitrary distance. This has been used by Riaud *et al.*<sup>69</sup> to synthesize bottle beams using swirling SAWs.

### 2. Radiation of a viscoacoustic wave by a surface wave propagating under a liquid

Surface waves not only feature a transverse vertical component, but also a longitudinal and a transverse horizontal component, both of which are tangential to the guiding surface. Therefore, they drive a shear motion in the fluid, which creates viscoacoustic waves that are attenuated within a microscopic viscoacoustic boundary layer. For a fluid of viscosity  $\mu$  and density  $\rho$ , the viscoacoustic boundary layer thickness reads  $\delta_{VE} = \sqrt{\frac{2\mu}{\rho\omega}}$ . Even though these waves do not propagate in the fluid, they can generate Rayleigh streaming.<sup>70</sup> For standing waves, Rayleigh streaming rolls penetrate the fluid up to approximately half an acoustic wavelength, whereas traveling waves can drive much larger Rayleigh streaming flow patterns.<sup>70</sup>

### 3. Leaky SAWs

When surface waves radiate a bulk wave into the liquid, the transverse vertical motion of the waves is severely damped, which results in a very fast attenuation of the wave (within approximately 10 wavelengths).<sup>31</sup> Although the radiated wave is very often used in acoustofluidics, the SAW attenuation due to the liquid loading

is a major limitation when designing SAW devices. It sets the actuation range of the device, which limits, for instance, the width of microfluidic channels or the size of acoustic tweezers. However, SAW attenuation has been used to detect the positions of sessile droplets<sup>71</sup> and to sort particles suspended in a fluid independently of the flow rate.<sup>72</sup> In the latter work by Ng *et al.*, two counter-propagating SAWs attenuate significantly through the channel, and the resulting field combines a standing and a traveling wave component. The amount of traveling wave decreases as one approaches the center of the channel. This creates a particle-size-dependent force competition between the radiation pressure of traveling and standing waves, which moves the largest particles toward the center of the channel while keeping the smallest ones near the walls.<sup>72</sup>

#### 4. Scholte waves

Scholte waves are longitudinal acoustic waves propagating at a fluid–solid interface and decaying exponentially in both directions along the normal to the interface.<sup>73</sup> Scholte waves do not radiate into the fluid, and therefore they dissipate very little energy and can propagate over a much longer distance than leaky Rayleigh waves. However, unlike TH waves such as BG and Love waves, they create a pressure field in the fluid, which enables radiation pressure and Rayleigh streaming but not Eckart streaming.<sup>74</sup> A peculiar characteristic of Scholte waves is that they should always exist<sup>73,75</sup> but are rarely observed. Indeed, Scholte waves and leaky Rayleigh waves are two linearly independent solutions of the same problem of a Rayleigh wave propagating under a fluid. Which solution dominates must therefore be determined by other means, such as the initial conditions when the wave enters the liquid.<sup>74</sup>

#### 5. Evanescent waves

Except for the viscoacoustic waves, all the waves presented so far have been propagative waves (with a real wavevector). The wavevector can also be imaginary. Taking the example of bulk waves in fluid, the wave vector must satisfy  $\omega^2/c^2 = k_r^2 + k_z^2$ . This is not always possible: for instance, small obstacles such as cavities at the

bottom of the solid,<sup>76</sup> sharp corners,<sup>77,78</sup> or pillars<sup>79</sup> can generate evanescent waves when forced to vibrate at frequencies low enough that the ultrasonic wavelength in the fluid is much larger than the size of these objects. Because the wave has such a large imaginary component, it decays sharply near the obstacle. This enables the trapping of much smaller particles than would have been possible with propagative waves, because (i) field gradients are much stronger, which enhances radiation pressure, and (ii) the field is confined to small regions of space, which eliminates cumulative effects such as Eckart streaming.

## IV. INTERDIGITATED TRANSDUCERS

An interdigitated transducer consists of two-parts: piezoelectric materials as substrate and patterned interdigitated electrodes [see Fig. 5(a)]. The fabrication of an IDT is detailed in a video by Mei *et al.*<sup>80</sup> The performance of these transducers is mainly determined by the piezoelectric substrate (see Sec. II) and the geometry of the electrodes. Here, we will distinguish between the subwavelength structure of the IDT (which has been extensively researched for telecommunication purposes), and the superstructure of the IDT over many wavelengths (which has been developing rapidly to address the needs of acoustofluidics). For a given superstructure, one can freely choose the subwavelength structure to achieve various degrees of balance between simplicity and efficiency.

### A. Subwavelength structure of IDTs

#### 1. Simple IDTs

Simple IDTs [see Fig. 6(a)] consist of periodic interdigitated electrodes deposited on the surface of a piezoelectric material. The wavelength of the SAW or the electric period of the gratings,  $\lambda_R$ , is defined by the periodicity of the finger pairs, such that the distance from one finger to the next is  $\lambda_R/4$  [see Fig. 5(b)]. The velocity of SAWs,  $V_R$ , depends on the material properties of the substrate, the propagation direction, and the thickness of the IDT. Consequently, the center frequency ( $f_0 = \omega/2\pi = c_R/\lambda_R$ ) of a given device

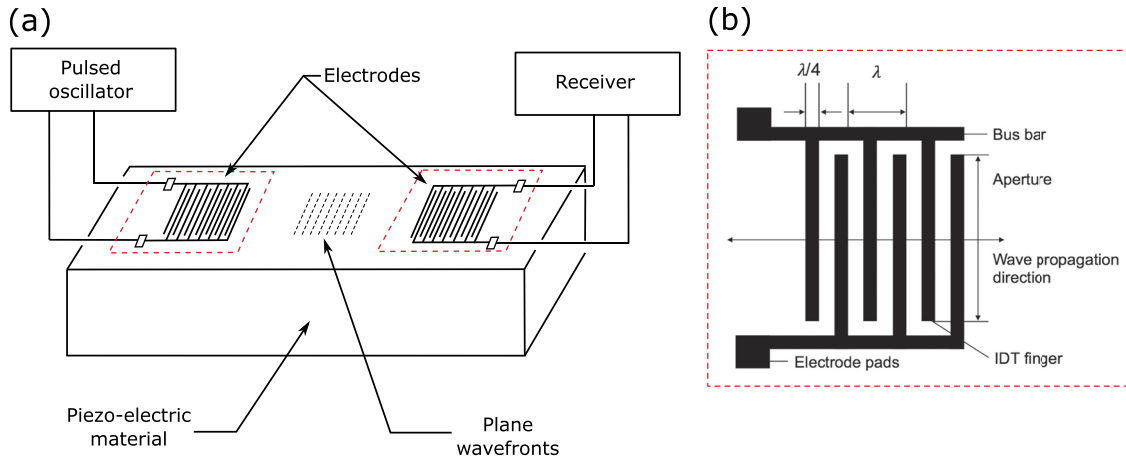
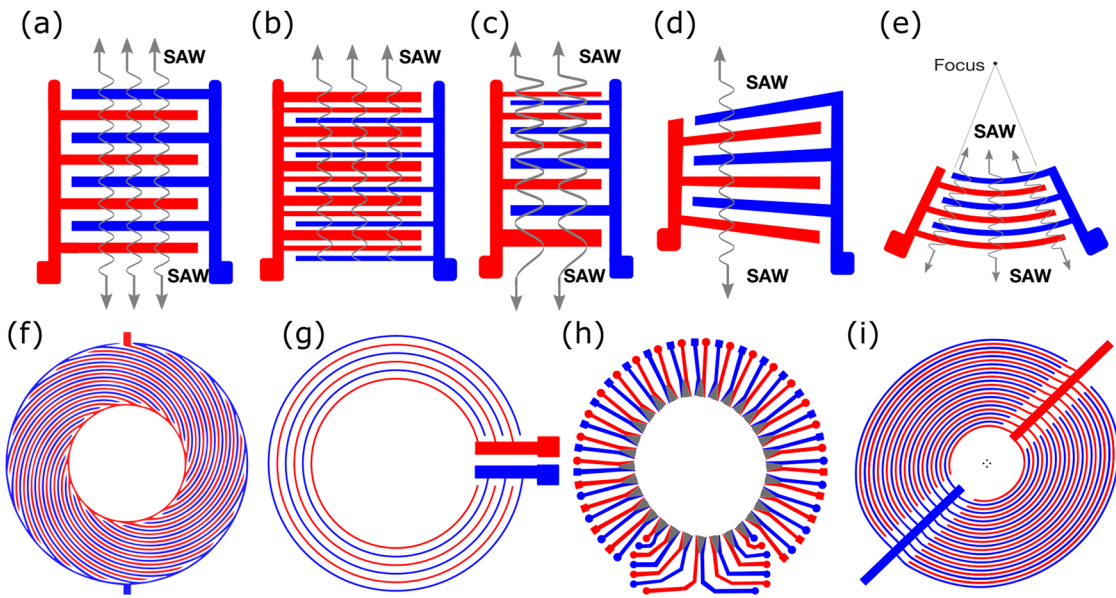


FIG. 5. (a) The first IDT as described by White and Voltmer in 1965.<sup>1</sup> (b) Typical electrode design and its parameters.<sup>7</sup>



**FIG. 6.** Interdigitated electrode designs for generating SAWs,<sup>81</sup> including (a) the original straight IDT with full-length finger electrode that is commonly used in telecommunication and microfluidics, (b) a single-phase unidirectional transducer for which the wave can only propagate along the setting direction, (c) a chirp IDT, (d) a slanted IDT, (e) a focus IDT. In contrast to the above IDT designs, the SAWs can travel from all directions with IDT designs such as (f) and (i) spiral IDTs,<sup>82,83</sup> (g) an annular IDT,<sup>52</sup> and (h) a circular IDT array.<sup>84</sup>

is determined by choice of substrate, propagation direction, and IDT design.

The admittance  $Y = 1/Z_e$  of an IDT is given by<sup>22</sup>

$$Y(\omega) = iC_T\omega + G_a(\omega) + B_a(\omega) \quad (11)$$

and the power radiated is

$$\langle \mathcal{P} \rangle = \frac{1}{2}G_a|U|^2. \quad (12)$$

The conductance and capacitance of straight IDT of width  $w$  with  $N$  finger pairs admits a simple expression useful to optimize the design of these transducers:

$$G_a(f) = 0.914\pi^2 K_R^2 C_T N f \left( \frac{\sin X}{X} \right)^2, \quad (13)$$

$$C_T = N(\epsilon_p + \epsilon_0)w, \quad (14)$$

$$X = \pi N \frac{f - f_0}{f_0}, \quad (15)$$

where  $K_R^2$  is the SAW electromechanical coupling coefficient of the substrate (see Table II),  $C_T$  is the static capacitance of the transducer,  $\epsilon_p = \sqrt{\epsilon_{11}\epsilon_{22} - \epsilon_{12}^2}$  is the effective permittivity in rotated coordinates,<sup>22</sup> and  $X$  is the reduced frequency of operation. When operating the IDT, the capacitance can be easily balanced by adding

a matched impedance (see Sec. II B)  $L_{\text{match}} = 1/(C_T\omega^2)$ . Therefore, matching to  $50 \Omega$  is achieved by ensuring that the conductance satisfies  $G_a = 0.02 \text{ S}$ . Assuming that the IDT width  $w$  is set by the microfluidic channel design, the number of fingers can be adjusted:

$$N = \sqrt{\frac{G_a}{0.914\pi^2 K_R^2 (\epsilon_p + \epsilon_0) w f_0}} \quad (16)$$

The bandwidth is then set by the number of fingers:

$$\text{BW} = \frac{\Delta f}{f_0} = \frac{0.635}{N}, \quad (17)$$

which indicates that additional fingers reduce the bandwidth. Furthermore, when using an IDT, individual fingers act as short circuits that feature an impedance mismatch with the incident wave. An order of magnitude of the reflection coefficient of one finger is  $r_e \approx \frac{\Delta Z}{Z} = \frac{\Delta V_R}{V_R} \approx \frac{1}{2}K_R^2$ . Therefore, for the lithium niobate Y-128 cut, the reflection coefficient approaches 2.5%, which limits the number of useful fingers to approximately 40.

When excited by a periodic signal, the IDT will generate SAWs owing to the inverse piezoelectric effect. Straight IDTs indiscriminately generate a pair of counter-propagating traveling SAWs. Therefore, at most half of the power provided to these IDTs is sent to the nearby channel, and the other half is wasted.

## 2. Unidirectional transducer

To reduce the energy loss of straight IDTs, electrode-width-controlled single-phase unidirectional transducers (SPUDTs)<sup>85</sup> can generate SAWs that propagate in just one direction [see Fig. 6(b)]. The cell of a conventional SPUDT consists of three fingers: two narrow electrodes and one wide electrode, whose widths are  $\lambda/8$  and  $\lambda/4$ , respectively.<sup>86</sup> The distance between the two narrow fingers is  $\lambda/8$ , and that between a narrow finger and the wide finger is  $3\lambda/16$ . Similar to straight IDTs, the reflection coefficient of individual fingers is of the order of  $r_e \approx \frac{1}{2}K_R^2$ , that is, around 2.5% for the Y-128 cut of LiNbO<sub>3</sub>. It is therefore necessary to use nearly 40 finger pairs to completely reflect a wave. When designing a device using SPUDTs to generate a standing wave (an SAW resonator), the concept of generation and reflection centers is important: they are located at the center of the hot electrode. For two SPUDTs facing each other, the generation centers of the transducers should be spaced by  $n\lambda_R$ , with  $n$  an integer.

Featuring a low energy loss and good directivity, SPUDTs are widely used in microfluidics when high ultrasonic power is needed.<sup>87,88</sup>

Other unidirectional transducer designs exist, including the distributed acoustic reflection transducer (DART),<sup>89</sup> the floating electrode unidirectional transducer (FUDT),<sup>90</sup> and the natural single-phase unidirectional transducer (NSPUDT).<sup>91</sup>

## B. Superstructure of IDTs

The subwavelength structure of the IDT determines the efficiency of the transducer. The superstructure (over many wavelengths) determines the acoustic field emitted by the transducer, which has become an important concern for acoustofluidic applications.

### 1. Straight IDTs

Straight IDTs are straight electrodes similar to the original design of White and Voltmer.<sup>1</sup> In the near field, they generate plane waves as wide as the transducer. They are the default choice of transducer for most acoustofluidic applications owing to their simplicity and the possibility of adjusting the transducer width. They can be combined with diffractive networks to create more advanced acoustic fields in microchannels<sup>66,67,76</sup> or with phononic structures in the solid to combine multiple functions by frequency multiplexing.<sup>18,19,92,93</sup> The IDT width should not be smaller than half a wavelength to prevent excessive diffraction. Instead, focused IDTs should be used to obtain narrow beams and spots.

### 2. Chirp IDTs

Chirp interdigitated transducers [see Fig. 6(c)] feature a gradually widening pitch.<sup>94</sup> This provides them with different resonance frequencies at different locations of the IDT, which results in a larger bandwidth (approximately 50%). According to Gabor's uncertainty principle, wideband actuation allows the generation of more finely detailed acoustic fields and therefore more precise particle manipulation. Such IDTs have been used to modulate the

acoustic wavelength in acoustic tweezers<sup>95</sup> and also to manipulate several microparticles selectively with time-modulated acoustic waves.<sup>96,97</sup> This type of application is likely to develop further in the future thanks to newly available theories of the radiation pressure for time-dependent signals.<sup>98</sup> The main limitation of chirp IDTs is their relatively complex design: the larger bandwidth complicates the impedance matching, undesired bulk waves may be generated, and backpropagating SAW waves can be reflected by the other fingers.

### 3. Slanted-finger IDTs

Slanted-finger IDTs (fan-shaped IDTs) feature a varying finger spacing across the width of the transducer [see Fig. 6(d)]. Unlike chirp IDTs, which generate overlapping SAWs with a broad range of frequencies, slanted-finger IDTs behave like a diffractive grating and generate narrow beams of SAWs with a frequency-dependent location. This allows fast, fine, and dynamic positioning of the SAW beam for droplet or cell actuation<sup>99,100</sup> and droplet splitting with surgical precision.<sup>101,102</sup> The concept has been extended to the use of circular slanted finger IDTs to enable adjustment of the propagation direction instead of the beam position.<sup>103,104</sup>

### 4. Focused IDTs

The goal of focused IDTs (FIDTs) is to maximize the SAW power over a small location (antenna gain). Circular FIDTs are suitable for isotropic substrates,<sup>46</sup> but also work reasonably well as local approximations of the wave surface for anisotropic substrates. However, the best performance is reached when the FIDT has the same shape as a section of the wave surface.<sup>105</sup> Focused transducers have been used extensively in micro-acoustofluidics to overcome capillary forces, for instance for droplet jetting<sup>87,106,107</sup> and atomization (nebulization),<sup>53</sup> and also to generate<sup>108,109</sup> and merge<sup>110</sup> droplets in microfluidic channels and create liquid bridges.<sup>111,112</sup> Other applications include mixing in microchannels<sup>113,114</sup> and droplets, ultra-fast particle concentration in droplets,<sup>115</sup> and high-throughput cell sorting.<sup>116</sup> The interested reader can consult Lei *et al.*<sup>117</sup> for an extensive review.

### 5. Annular IDTs

Annular IDTs can generate a focused acoustic field from all directions [see Fig. 6(g)]. These transducers maximize the SAW power within the smallest possible region (antenna gain), which is especially important when considering nonlinear phenomena. The design of annular IDTs (and spiraling IDTs) imposes much tighter tolerances than that of focused IDTs, because the wave field is fully specified by the IDT geometry. Unlike focused IDTs, where design errors would result in slightly worse focusing, a failed design of annular IDT would result in destructive interferences and much poorer performance. On isotropic substrates, annular transducers are simply a series of concentric circles,<sup>52</sup> whereas their shape is more elaborate on anisotropic substrates.<sup>39</sup> If the piezoelectric coupling coefficient has the same sign over all the propagation directions, annular IDTs must have the same shape as the wave surface.

The high power of annular transducers makes them especially promising for the most power-intensive applications, such as droplet jetting and liquid pipetting.<sup>52</sup> A key difference with FIDTs is that annular transducers ensure an axisymmetric acoustic field (and acoustic forces) in the droplet,<sup>52</sup> which is not possible with FIDTs. However, pairs of FIDTs can be independently controlled to adjust the direction of the droplet jet.<sup>107</sup>

## 6. Spiraling IDTs

Spiraling IDTs generate waves that rotate around a fixed point. These waves (swirling SAWs) carry an orbital angular momentum that can be transmitted to a droplet or fluid placed upon them,<sup>118</sup> for instance to achieve droplet centrifuging.<sup>82</sup> In addition, destructive interference between incoming wavefronts at the fixed point means that the wave amplitude vanishes,<sup>118</sup> which is essential for particle trapping.<sup>15</sup> Spiraling IDTs [see Fig. 6(i)] have been designed specifically to synthesize swirling SAWs.<sup>83</sup>

The size of the dark region (and the orbital angular momentum) of a swirling SAW is proportional to the number of branches of the spiraling transducer. Therefore, designs for high orbital angular momentum use a different interconnect to accommodate many branches [see Fig. 6(f)].<sup>82</sup>

Similar to annular transducers, spiraling transducers are extremely sensitive to design errors, and anisotropy must be carefully considered.<sup>83,119</sup> However, Lamb waves exhibit good piezoelectric coupling and are approximately isotropic,<sup>46</sup> which allows the synthesis of swirling SAWs using a simple spiral.<sup>45</sup>

Finally, the spiral can be used to generate bulk waves instead of surface waves.<sup>45</sup> Instead of the Archimedean spiral (constant pitch) of conventional transducers, these new transducers use a Archimedes–Fermat spiral (varying pitch) to integrate a focusing function. They have recently been used to achieve the first acoustic tweezers manipulation of a single human cell with extreme precision.<sup>120</sup>

## 7. Arrays of IDTs

Arrays of IDTs can be used in a very similar fashion to transducer arrays.<sup>9</sup> The main challenge is to combine interfering wave fields from all sides, which, similarly to annular and spiraling transducers, places very stiff constraints on the field that can be synthesized. Riaud *et al.*<sup>40</sup> have developed a spectral inverse filter method to control an array of 32 IDTs that can synthesize a large number of wave fields [see Fig. 6(h)], including plane waves, focused waves, and swirling SAWs, and achieve several of the elementary acoustofluidic functions, such as droplet displacement, splitting, merging, and atomization.<sup>84</sup>

## V. SIMULATION OF COMPLEX FIELDS

The need for increasingly complex transducers has stimulated the development of new design tools to predict their performance. These can essentially be classified into three methods with increasing generality at the expense of increasingly large memory requirements: (i) simulation of a line source on a surface, (ii) simulation of a three-dimensional field emitted from a flat surface, and (iii) full three-dimensional simulations.

In all cases, the simulated entity must be discretized to satisfy Shannon's principle (at least two mesh elements per wavelength, which in practice turns out to be six or more elements per wavelength). This sets the memory requirements.

### A. Simulation of three-dimensional acoustic fields

#### 1. Finite element method

Three-dimensional simulations based on the finite element method (FEM) are among the most widely used and versatile IDT design tools. They are indispensable to simulate devices where the propagation medium is not homogeneous (such as when it includes gradients of material properties or defects). These methods are the simplest to set up, but also the most expensive numerically. Indeed, discretization at six elements per wavelength requires 3400 elements per cubic wavelength in three dimensions, and the three-dimensional mechanical motion of the wave with the associated electric potential using a second-order discretization scheme then requires 60 000 degrees of freedom per cubic wavelength. Consequently, the simulation of a  $2 \times 2 \text{ mm}^2$  SAW device operating at 20 MHz ( $\lambda = 200 \mu\text{m}$ ) requires 6 000 000 degrees of freedom, that is, nearly 192 GB, to store only the solution vector for such a small device (irrespective of the solver used). Therefore, three-dimensional simulations quickly become impractical, especially for large transducers such as focused<sup>121</sup> or spiraling<sup>119</sup> transducers. Luckily, the fluid loading has a limited impact on the surface wave propagation. This allows simulation of the acoustic field in the fluid using a perturbation approach where the acoustic field on the solid surface is simulated first and the radiated field is then computed by assuming that the fluid medium is unbounded.

### B. Simulation of bulk waves radiating from a surface into an infinite half-space

#### 1. Angular spectrum method

The angular spectrum method is one of the simplest and most efficient ways to simulate acoustic waves in a homogeneous three-dimensional half-space. Half-space means that no boundary exists and the waves sent from some source surface are allowed to propagate to infinity.

Given a vertical vibration  $u(\mathbf{r})$  at the plane  $z = 0$ , the angular spectrum method reconstructs the field using the dispersion relation of the wave. The idea is that the incident field can be seen as a combination of plane waves:

$$u(\mathbf{r}) = e^{-i\omega t} \int_{k_x} \int_{k_y} U(k_x, k_y) e^{ik_x x + ik_y y + ik_z(k_x, k_y) z} dk_x dk_y. \quad (18)$$

The value of  $U$  is obtained from the two-dimensional spatial Fourier transform of  $u$  at  $z = 0$  (angular spectrum). The value of  $k_z(k_x, k_y)$  is obtained from the dispersion relation, which reads  $k_x^2 + k_y^2 + k_z^2 = k^2 = \omega^2/V^2$  in an isotropic medium. The method is exactly the same when the medium is anisotropic, except that the calculation becomes more cumbersome because the wave velocity  $V(\psi, \phi)$  now depends on the direction of propagation, with  $(\psi, \phi)$  the propagation angles.

The Fourier transform of  $u$  and the integral in Eq. (18) can be computed very efficiently using two-dimensional direct and inverse fast Fourier transforms.<sup>45,122</sup> The main limitation of the method is

that it becomes impractical when the emitting surface is not flat. In this case, the boundary element method is more suitable.

## 2. Boundary element method

In the angular spectrum method, the field is resolved as a combination of plane waves. Another approach is to resolve the emitting surface as a combination of point sources. This works best when there are not many sources, but it can also replace the angular spectrum if the points are distributed on a curved surface or in three-dimensional space. The field emitted by a point source sensed at some probe point is called the Green function. The Green function theory is derived to include dependence on boundary conditions, but is mainly useful when considering an infinite homogeneous medium. In this case, the boundary conditions are the same for all source points, and the Green function is greatly simplified.

The Coulomb potential of a point charge is one of the best known example of a Green function. The total electric field is simply the combination of the electric field from each point charge. The same holds true for the Green function of acoustic waves. For isotropic waves, the Green function of the acoustic potential emitted by a surface element with normal vibration  $V_n$  sensed at a distance  $R$  has the simple expression<sup>22</sup>

$$\varphi = e^{i\omega t} V_n \frac{e^{-ikR}}{2\pi R}, \quad (19)$$

where  $k$  is the wavenumber. The velocity and pressure can be deduced from  $\varphi$  as  $v = -\nabla\varphi$  and  $p = \rho_0 \partial_t \varphi$ .

The acoustic field radiated by a vibrating surface  $A$  is computed using the Rayleigh integral:

$$\varphi = e^{i\omega t} \iint_A V_n \frac{e^{-ikR}}{2\pi R} dA. \quad (20)$$

Anisotropic materials also admit Green functions, as long as they are homogeneous. These Green functions are generally non-trivial, but can be obtained using the stationary phase approximation.<sup>123</sup> Boundary element methods have been used in the design of diffractive elements in acoustofluidic devices.<sup>68</sup>

## C. Simulation of surface waves radiating from a line

When working with SAWs, the wave is embedded in a two-dimensional propagation plane. The IDT can be seen as a series of lines, which are generally curved. Therefore, the acoustic field generated by an IDT is best computed using the two-dimensional analogs

of Green functions. Such a Green function for the field sensed at a location  $R$  from a source point has been derived by Laude *et al.*,<sup>124</sup> and its simplified expression in the far field<sup>39</sup> is extremely useful when designing complex IDTs:

$$G(R) \approx \frac{Aa(\bar{\psi}) \exp[-i\omega Rh(\bar{\psi}) - i(\pi/4)\text{sign}(h''(\bar{\psi}))]}{\sqrt{\omega R|h''(\bar{\psi})|}}, \quad (21)$$

where  $h(\psi) = k(\bar{\psi}) \cdot R/\omega$  is the angular dependence of the wave phase. With this Green function it is possible to find the direction of propagation of the wave energy  $\bar{\psi}$ , which differs from the direction of propagation of the wave phase owing to the beam-stirring effect in anisotropic media.  $\bar{\psi}$  is solution of the stationary phase differential equation  $dh/d\bar{\psi} = 0$ . The coefficient  $a(\bar{\psi})$  indicates the electromechanical conversion of the wave for a direction of propagation  $\bar{\psi}$ <sup>124</sup> and can be obtained using a simple two-dimensional model of a straight IDT. This method has been used to design focused IDTs<sup>125</sup> and spiraling transducers.<sup>118</sup>

A method analogous to the angular spectrum has also been proposed by Wu *et al.*,<sup>126</sup> but it does not yet account for the anisotropy of the piezoelectric coupling and especially changes of phase in this coefficient, which can yield erroneous results. Therefore, additional work is needed to make this exciting development more reliable.

## VI. CHARACTERIZATION METHODS

IDTs reversibly convert electric signals into acoustic waves. Therefore, they should be characterized both from an electrical and from an acoustic standpoint. In this section, we review several characterization methods and their relevance for acoustofluidics. These methods are summarized in Table III.

### A. Electrical characterization

#### 1. Multimeter

Multimeters are cheap hand-held instruments that allow checking the working of IDTs on the fly. Performing some essential safety checks of the experimental setup using a multimeter can avoid damage to the power generator due to a mismatched load. These checks include (i) checking for short circuits on the IDT by probing the contact pads, (ii) checking the IDT capacitance by probing the contact pads, and (iii) checking for an open circuit by probing the connection between the cables and the contact pads of the IDT.

TABLE III. Methods for the characterization of acoustic fields.

Method	Training time	Instrument cost	Measurement speed	Qualitative/quantitative
Hydrophone	Average	Average	Slow	Quantitative
Laser vibrometer	Intensive	High	Fast	Quantitative
Small particles	Intensive	Low	Medium	Semiquantitative
Dust particles	Few	Low	Extremely fast	Qualitative
Thermal imaging	Few	Low	Fast	Qualitative
Brillouin scattering	Intensive	High	Slow	Semiquantitative

## 2. Voltage standing wave ratio meter

Voltage standing wave ratio (VSWR) meters are easy-to-use instruments designed to measure the mismatch between a transmission line (coaxial cable) and a load (typically an antenna), as indicated by the VSWR. They include a directional coupler that allows them to distinguish between electromagnetic waves traveling forward and backward in the coaxial cable. They also feature very low insertion loss (<1 dB), which allows them to be kept plugged into the line during the experiment.

Most VSWR meters display the forward and backward power (“reflected power”). It is worth noting that, similarly to antennas, IDTs can receive SAWs and convert them back into electric power. In this regard, the reflected power displayed by VSWR meters is not only due to mismatch of electrical impedance, but also possibly due to ultrasonic reflections. Nevertheless, VSWR meters are among the easiest-to-use instruments to check the power supplied to the IDT and the impedance matching.

## 3. Vector network analyzer

Vector network analyzers (VNAs) are high-end characterization instruments to measure the scattering parameters (S-parameters) of linear circuits.<sup>127</sup> The  $s_{11}$  coefficient of the scattering matrix is the complex reflection coefficient  $\Gamma$  of the load, and can be related to its electrical impedance using Eq. (8):

$$Z_e = 50\Omega \frac{s_{11} + 1}{1 - s_{11}}. \quad (22)$$

Knowing the impedance of the transducer makes it possible to match it to improve power transfer and protect the power generator.

VNAs also allow one to locate the resonance frequency of the transducer, which appears as a minimum of the reflection coefficient (or as a peak in the resistance of the transducer). The main drawbacks of VNAs are their high cost and difficult operation, which requires some training.

A note of caution is that VNAs are typically used with assigned cables (or needles). Changing these connectors requires recalibrating the instrument. Furthermore, the impedance is measured up to the tip of the connectors, and therefore the load considered by the VNA (and the displayed  $s_{11}$ ,  $Z_e$ , and so on) are those of the transducer and anything in between up to the tip of the VNA connector. Therefore, the impedance matching must then be done at the location where the tip of the VNA connector was inserted.

## B. Characterization of the acoustic field

### 1. Quantitative methods

Quantitative knowledge of the acoustic field allows troubleshooting of the IDT design and facilitates the analysis of acoustofluidic experiments. Older methods used ingenious systems based on light bulbs connected to microphones to visualize the acoustic field using photographic cameras.<sup>128</sup> Nowadays, the acoustic field pressure can be measured using a hydrophone, or the vibration can be measured using a laser vibrometer.<sup>22</sup>

*a. Hydrophone.* Hydrophones include a piezoelectric element to measure the intensity of acoustic fields in liquids. The size of the sensing element must be smaller than half a wavelength to minimize directivity issues, which limits the sensitivity of measurement. To

measure an acoustic field, the hydrophone must be moved in space. This requires a mechanical motion, which requires precision motors and is prone to vibrations. Overall, hydrophones are easy to use and relatively affordable, but their operation is slow. The directivity problem also limits hydrophones to frequencies below 20 MHz.

*b. Laser vibrometer.* Laser vibrometry uses an optical interferometry setup to probe the mechanical displacement of a surface.<sup>129</sup> The surface can be a thin film (such as a Mylar film), which allows measurements of cross-sections of the acoustic film in a liquid.<sup>130</sup> Vibrometers provide quantitative measurements of the acoustic field, and they can scan vibrating surfaces either by moving them with motors or using a system of motorized mirrors to move the measurement beam. The small mass of the mirrors means vibrations are damped much faster so that the vibrometer’s scanning time is much shorter than when using a hydrophone. The resolution of a vibrometer is limited by the size of the optical spot that can be formed on the measured surface, which is of the order of 1 μm. They feature a much larger bandwidth than hydrophones and have a minimal effect on the measured acoustic waves. Indeed, for a perfectly reflective surface, only the radiation pressure of light influences the acoustic field, which is exactly the lowest bound allowed by the Heisenberg uncertainty principle (interested readers can refer to the work of Brillouin on Maxwell’s demon for a rigorous discussion<sup>131</sup>).

There is a considerable freedom in designing vibrometers, depending on the experimenter’s needs. The simplest vibrometers use a stabilized Michelson design where the reference arm has a feedback loop to maintain maximum contrast.<sup>132</sup> This provides a very wide bandwidth to these vibrometers, but the setup is tedious and the feedback loop is difficult to implement. More specialized heterodyne Mach–Zehnder vibrometers use an acousto-optic modulator to induce a frequency shift between the measurement and reference arms.<sup>133</sup> They are much easier to set up, but have a bandwidth limited by the frequency of the modulator. State-of-the-art vibrometers can measure the vibrations of rough surfaces<sup>134</sup> with gigahertz bandwidth<sup>135</sup> and require little adjustment, but are expensive instruments.

### 2. Qualitative methods

The following methods are classified as qualitative because they do not offer a direct readout of the acoustic field amplitude and phase. Nevertheless, some of them can become quantitative provided that some additional post-processing steps are taken.

*a. Small particles suspended in a fluid.* When the acoustic field to be measured is known in advance (e.g., in high-quality resonators), its magnitude can be measured using acoustofluidic phenomena such as acoustic streaming or acoustic radiation pressure. One of the best example of such an approach is the tracking of particles to estimate the radiation pressure on them and deduce the acoustic energy density.<sup>136</sup> A similar approach has also been applied to radiation pressure and Eckart streaming.<sup>137</sup> While this method is experimentally simple, it requires extensive preparation (numerical simulations), well-controlled experiments, and extensive postprocessing. In most experiments, the particle trajectories are processed using general defocusing particle tracking,<sup>138</sup> which allows reconstruction of their three-dimensional trajectories.

*b. Dust.* Fine sticky dust (such as cigarette smoke) can be used to visualize the spatial distribution of SAW energy within a few seconds with a resolution of a few tens of micrometers.<sup>139</sup> Similar to Chladni plates, it reveals the presence of nodes and antinodes, but is not quantitative.

*c. Thermal imaging.* When an acoustic wave is absorbed, its energy is converted to heat, which can increase the temperature of materials as it accumulates. This allows visualization of the spatial distribution of ultrasonic beam intensity. A first approach is through direct use of a thermal camera,<sup>140</sup> but not only are these cameras expensive, they also do not work well across all materials, for instance glass blocks infrared radiation. An alternative is to use thermochromic sheets of liquid crystals,<sup>141,142</sup> which can reveal cross-sections of the acoustic beam power. By positioning a thermochromic sheet at different heights, it is possible to record a three-dimensional view of the acoustic field.<sup>141</sup> While the method is cheap, fast, and visually appealing, it is sensitive to the beam intensity (and not the pressure), its resolution is low, and the magnitude of temperature change depends not only on the incident beam power but also on the heat transfer from the thermochromic sheet to the ambient fluid, which is difficult to control. It is therefore challenging to extract quantitative information with this method.

*d. Brillouin scattering.* Sound propagation changes the density and temperature of the propagation medium, which in turn changes its refractive index proportionally to the variation in density.<sup>22,143</sup> The diffraction of light by acoustic waves (mediated by changes in refractive index) is called Brillouin scattering. The diffraction effect is generally small, but can be observed using interferometric methods, for instance schlieren imaging. A beautiful demonstration has been given by Crockett and Rueckner.<sup>144</sup> What makes Brillouin scattering especially attractive is that it is valid for any electromagnetic waves, including x-rays. The latter feature good transmission across solids, and their very short diffraction limit allows very high resolution and opens new avenues for nondestructive control and ultrasonic characterization of materials.<sup>145</sup> Another exciting direction is the use of optical phase contrast microscopy instead of schlieren imaging, which could allow direct observation of the microscale acoustic fields of acoustofluidic devices.<sup>146</sup> Time-dependent acoustic wave propagation can be observed using stroboscopic imaging.

The main problem with Brillouin scattering is that the primary measured quantity is the light intensity, which indicates the deflection of the light instead of the refractive index. The deflection is proportional to the magnitude of the gradient of refractive index, and therefore does not yield the sign of the change of the refractive index (it is not possible to know if the material expanded or compressed).<sup>144</sup> This problem can be addressed by using optical filters<sup>144</sup> to detect the direction of the deflection. Nevertheless, this provides the change in refractive index, not the mechanical displacement. The latter can be inferred through additional assumptions by solving an inverse problem.<sup>145</sup>

*e. Scanning electron microscopy.* When an acoustic wave propagates in a piezoelectric solid, it creates an electric field that can deflect an electron beam. Similar to Brillouin scattering, scanning electron microscopes can record images of acoustic waves in piezoelectric solids, with a resolution even higher than x-rays.<sup>46,147</sup> While in principle the electric potential associated with the wave could

be reconstructed in a similar fashion to the refractive index when using light waves, limitations remain on obtaining the mechanical displacement.

## VII. PERSPECTIVES

In this review, we have described how new applications of acoustofluidics have changed the focus of IDT design from simple delay lines to transducers geared to synthesize much more complex acoustic fields.

### A. Current limitations

In the authors' opinion, interdigitated transducers for acoustofluidic applications suffer from two main limitations: (i) they are not reconfigurable and (ii) they are difficult to design and implement. These two problems are interrelated: because IDT arrays are not reconfigurable, they must be designed specifically for each application. However, the design of acoustofluidic devices in general, and especially IDTs, is not straightforward, and therefore each application requires a considerable amount of work. This restricts the adoption of IDT-based acoustofluidic to a small community. Reconfigurable IDT arrays<sup>40</sup> and rapid prototyping methods<sup>148,149</sup> exist, but the former rely on state-of-the-art field-programmable gate arrays (FPGAs) with cumbersome electrical connections, and the latter have a limited refreshing rate (so only a few devices can be tested each day). Conversely, IDT performance can be estimated using home-made numerical simulations based on finite elements or Green functions, but this requires a considerable investment in research and training before valuable results can be obtained.

### B. Future improvements

This high barrier of entry to the field may discourage researchers from related field who would otherwise have been interested in acoustofluidic applications. While it can be addressed by simplifying device design, it is the authors' opinion that this would be a simplistic solution. Instead, standardization of acoustofluidic chips for any given function is expected to emerge naturally as research progresses. In this regard, comparing various chip design and their performance using common standards appears to be a crucial step in this direction. Furthermore, the development of specialized radiofrequency signal generators able to automatically adjust their frequency<sup>150,151</sup> and match their impedance to the load looks highly desirable. Finally, open-source codes to compute the acoustic field generated by IDTs could facilitate the integration of new research groups into the acoustofluidic community.

### C. Emerging applications

The wide variety of IDTs is likely to prompt renewed interest in design tools and characterization methods for SAW fields. It is also likely that these more advanced transducers will be of benefit to other fields such as telecommunications and optical displays<sup>143,152</sup> and quantum computing.<sup>2</sup>

## ACKNOWLEDGMENTS

This work was supported by the National Natural Science Foundation of China under Grant Nos. 12004078 and 61874033,

the State Key Lab of ASIC and Systems, the Science and Technology Commission of Shanghai Municipality Award/Grant Nos. 22QA1400900 and 22WZ2502200, and Fudan University 2021MS001, 2021MS002 and 2020KF006.

## AUTHOR DECLARATIONS

### Conflict of Interest

The authors declare no competing interests.

## DATA AVAILABILITY

Data sharing not applicable to this article as no datasets were generated or analyzed during the current study.

## REFERENCES

- <sup>1</sup>White, RM, Voltmer, FW. Direct piezoelectric coupling to surface elastic waves. *Appl Phys Lett* 1965;7(12):314–316. <https://doi.org/10.1063/1.1754276>.
- <sup>2</sup>Delsing, P, Cleland, AN, Schuetz, MJA, Knörzer, J, Giedke, G, Cirac, JI, Srinivasan, K, Wu, M, Balram, KC, Bäuerle, C, et al. The 2019 surface acoustic waves roadmap. *J Phys D Appl Phys* 2019;52(35):353001. <https://doi.org/10.1088/1361-6463/ab1b04>.
- <sup>3</sup>Shiokawa, S, Matsui, Y, Moriizumi, T. Experimental study on liquid streaming by SAW. *Jpn J Appl Phys* 1989;28(S1):126. <https://doi.org/10.7567/jjaps.28s1.126>.
- <sup>4</sup>Bruus, H, Dual, J, Hawkes, J, Hill, M, Laurell, T, Nilsson, J, Radel, S, Sadhal, S, Wiklund, M. Forthcoming Lab on a Chip tutorial series on acoustofluidics: Acoustofluidics—Exploiting ultrasonic standing wave forces and acoustic streaming in microfluidic systems for cell and particle manipulation. *Lab Chip* 2011;11(21):3579–3580. <https://doi.org/10.1039/c1lc90058g>.
- <sup>5</sup>Winkler, A, Brünig, R, Faust, C, Weser, R, Schmidt, H. Towards efficient surface acoustic wave (SAW)-based microfluidic actuators. *Sens Actuators A* 2016;247:259–268. <https://doi.org/10.1016/j.sna.2016.06.006>.
- <sup>6</sup>Friend, J, Yeo, LY. Microscale acoustofluidics: Microfluidics driven via acoustics and ultrasonics. *Rev Mod Phys* 2011;83(2):647. <https://doi.org/10.1103/revmodphys.83.647>.
- <sup>7</sup>Connacher, W, Zhang, N, Huang, A, Mei, J, Zhang, S, Gopesh, T, Friend, J. Micro/nano acoustofluidics: Materials, phenomena, design, devices, and applications. *Lab Chip* 2018;18(14):1952–1996. <https://doi.org/10.1039/C8LC00112J>.
- <sup>8</sup>Rezk, AR, Ahmed, H, Ramesan, S, Yeo, LY. High frequency sonoprocessing: A new field of cavitation-free acoustic materials synthesis, processing, and manipulation. *Adv Sci* 2021;8(1):2001983. <https://doi.org/10.1002/advs.202001983>.
- <sup>9</sup>Drinkwater, BW. Dynamic-field devices for the ultrasonic manipulation of microparticles. *Lab Chip* 2016;16(13):2360–2375. <https://doi.org/10.1039/c6lc00502k>.
- <sup>10</sup>Kolesnik, K, Xu, M, Lee, PVS, Rajagopal, V, Collins, DJ. Unconventional acoustic approaches for localized and designed micromanipulation. *Lab Chip* 2021;21:2837. <https://doi.org/10.1039/d1lc00378j>.
- <sup>11</sup>Fu, YQ, Luo, JK, Du, XY, Flewitt, AJ, Li, Y, Markx, GH, Walton, AJ, Milne, WI. Recent developments on ZnO films for acoustic wave based bio-sensing and microfluidic applications: A review. *Sens Actuators B* 2010;143(2):606–619. <https://doi.org/10.1016/j.snb.2009.10.010>.
- <sup>12</sup>Rufo, J, Cai, F, Friend, J, Wiklund, M, Huang, TJ. Acoustofluidics for biomedical applications. *Nat Rev Methods Primers* 2022;2(1):30. <https://doi.org/10.1038/s43586-022-00109-7>.
- <sup>13</sup>Baudoin, M, Thomas, J-L. Acoustic tweezers for particle and fluid micro-manipulation. *Annu Rev Fluid Mech* 2020;52:205–234. <https://doi.org/10.1146/annurev-fluid-010719-060154>.
- <sup>14</sup>Courtney, CRP, Drinkwater, BW, Demore, CEM, Cochran, S, Grinenko, A, Wilcox, PD. Dexterous manipulation of microparticles using Bessel-function acoustic pressure fields. *Appl Phys Lett* 2013;102(12):123508. <https://doi.org/10.1063/1.4798584>.
- <sup>15</sup>Baresch, D, Thomas, JL, Marchiano, R. Observation of a single-beam gradient force acoustical trap for elastic particles: Acoustical tweezers. *Phys Rev Lett* 2016;116(2):024301. <https://doi.org/10.1103/PhysRevLett.116.024301>.
- <sup>16</sup>Wu, H, Tang, Z, You, R, Pan, S, Liu, W, Zhang, H, Li, T, Yang, Y, Sun, C, Pang, W, et al. Manipulations of micro/nanoparticles using gigahertz acoustic streaming tweezers. *Nanotechnol Precis Eng* 2022;5(2):023001. <https://doi.org/10.1063/10.0009954>.
- <sup>17</sup>Antfolk, M, Laurell, T. Continuous flow microfluidic separation and processing of rare cells and bioparticles found in blood—A review. *Anal Chim Acta* 2017;965:9–35. <https://doi.org/10.1016/j.aca.2017.02.017>.
- <sup>18</sup>Wilson, R, Reboud, J, Bourquin, Y, Neale, SL, Zhang, Y, Cooper, JM. Phononic crystal structures for acoustically driven microfluidic manipulations. *Lab Chip* 2011;11(2):323–328. <https://doi.org/10.1039/c0lc00234h>.
- <sup>19</sup>Li, F, Cai, F, Zhang, L, Liu, Z, Li, F, Meng, L, Wu, J, Li, J, Zhang, X, Zheng, H. Phononic-crystal-enabled dynamic manipulation of microparticles and cells in an acoustofluidic channel. *Phys Rev Appl* 2020;13(4):044077. <https://doi.org/10.1103/physrevapplied.13.044077>.
- <sup>20</sup>Mason, WP, Thurston, RN, ed. *Physical acoustics*. New York: Academic Press. 1981. Vol. 15.
- <sup>21</sup>Campbell, C. *Surface acoustic wave devices and their signal processing applications*. Elsevier. 2012.
- <sup>22</sup>Royer, D, Dieulesaint, E. *Elastic waves in solids II: Generation, acousto-optic interaction, applications*. Springer Science & Business Media. 1999.
- <sup>23</sup>Huang, A, Connacher, W, Stambaugh, M, Zhang, N, Zhang, S, Mei, J, Jain, A, Alluri, S, Leung, V, Rajapaksa, AE, et al. Practical microcircuits for handheld acoustofluidics. *Lab Chip* 2021;21(7):1352–1363. <https://doi.org/10.1039/dlc01008a>.
- <sup>24</sup>Strobl, CJ, Schäflein, C, Beierlein, U, Ebbecke, J, Wixforth, A. Carbon nanotube alignment by surface acoustic waves. *Appl Phys Lett* 2004;85(8):1427–1429. <https://doi.org/10.1063/1.1787159>.
- <sup>25</sup>Ma, Z, Guo, J, Liu, YJ, Ai, Y. The patterning mechanism of carbon nanotubes using surface acoustic waves: The acoustic radiation effect or the dielectrophoretic effect. *Nanoscale* 2015;7(33):14047–14054. <https://doi.org/10.1039/c5nr04272k>.
- <sup>26</sup>Zhang, P, Rufo, J, Chen, C, Xia, J, Tian, Z, Zhang, L, Hao, N, Zhong, Z, Gu, Y, Chakrabarty, K, et al. Acoustoelectronic nanotweezers enable dynamic and large-scale control of nanomaterials. *Nat Commun* 2021;12(1):3844. <https://doi.org/10.1038/s41467-021-24101-z>.
- <sup>27</sup>Campbell, C. *Surface acoustic wave devices for mobile and wireless communications, four-volume set*. Academic Press. 1998.
- <sup>28</sup>Lewis, M. Surface skimming bulk wave, SSBW. 1977 *Ultrasonics Symposium*. IEEE. 1977. pp. 744–752.
- <sup>29</sup>Every, AG, Maznev, AA, Grill, W, Pluta, M, Comins, JD, Wright, OB, Matsuda, O, Sachse, W, Wolfe, JP. Bulk and surface acoustic wave phenomena in crystals: Observation and interpretation. *Wave Motion* 2013;50(8):1197–1217. <https://doi.org/10.1016/j.wavemoti.2013.02.007>.
- <sup>30</sup>Rayleigh, Lord. On waves propagated along the plane surface of an elastic solid. *Proc London Math Soc* 1885;s1-17(1):4–11. <https://doi.org/10.1112/plms/s1-17.1.4>.
- <sup>31</sup>Campbell, JJ, Jones, WR. Propagation of surface waves at the boundary between a piezoelectric crystal and a fluid medium. *IEEE Trans Sonics Ultrason* 1970;17(2):71–76. <https://doi.org/10.1109/tsu.1970.7404095>.
- <sup>32</sup>Thurston, RN, Pierce, AD, Papadakis, EP. *Reference for modern instrumentation, techniques, and technology: Ultrasonic instruments and devices I: Ultrasonic instruments and devices I*. Academic Press. 1998.
- <sup>33</sup>Shibayama, K, Yamanouchi, K, Sato, H, Meguro, T. Optimum cut for rotated Y-cut LiNbO<sub>3</sub> crystal used as the substrate of acoustic-surface-wave filters. *Proc IEEE* 1976;64(5):595–597. <https://doi.org/10.1109/proc.1976.10181>.
- <sup>34</sup>Campbell, CK. Applications of surface acoustic and shallow bulk acoustic wave devices. *Proc IEEE* 1989;77(10):1453–1484. <https://doi.org/10.1109/5.40664>.

- <sup>35</sup>Čiplys, D, Rimeika, R. Electromechanical coupling coefficient for surface acoustic waves in proton exchanged 128°-rotated Y-cut lithium niobate. *Appl Phys Lett* 1998;73(17):2417–2419. <https://doi.org/10.1063/1.122452>.
- <sup>36</sup>Soluch, V, Lysakowska, M. Surface acoustic waves on X-cut LiNbO<sub>3</sub>. *IEEE Trans Ultrason Ferroelectr Freq Control* 2005;52(1):145–147. <https://doi.org/10.1109/tuffc.2005.1397360>.
- <sup>37</sup>Hickernell, FS. -3- Surface acoustic wave technology macrosuccess through microseisms. *Phys Acoust* 1999;24:135–207. [https://doi.org/10.1016/s0893-388x\(99\)80025-6](https://doi.org/10.1016/s0893-388x(99)80025-6).
- <sup>38</sup>Zhang, N, Mei, J, Gopesh, T, Friend, J. Optimized, omnidirectional surface acoustic wave source: 152°Y-rotated cut of lithium niobate for acoustofluidics. *IEEE Trans Ultrason Ferroelectr Freq Control* 2020;67(10):2176–2186. <https://doi.org/10.1109/tuffc.2020.2993766>.
- <sup>39</sup>Laude, V, Gérard, D, Khelfaoui, N, Jerez-Hanckes, CF, Benchabane, S, Khelif, A. Subwavelength focusing of surface acoustic waves generated by an annular inter-digital transducer. *Appl Phys Lett* 2008;92(9):094104. <https://doi.org/10.1063/1.2891055>.
- <sup>40</sup>Riaud, A, Thomas, J-L, Charron, E, Bussonnière, A, Matar, OB, Baudoin, M. Anisotropic swirling surface acoustic waves from inverse filtering for on-chip generation of acoustic vortices. *Phys Rev Appl* 2015;4(3):034004. <https://doi.org/10.1103/physrevapplied.4.034004>.
- <sup>41</sup>Lamb, H. On the vibrations of an elastic sphere. *Proc London Math Soc* 1881;s1-13(1):189–212. <https://doi.org/10.1112/plms/s1-13.1.189>.
- <sup>42</sup>Rezk, AR, Tan, JK, Yeo, LY. HYbriD Resonant Acoustics (HYDRA). *Adv Mater* 2016;28(10):1970–1975. <https://doi.org/10.1002/adma.201504861>.
- <sup>43</sup>Moroney, RM, White, RM, Howe, RT. Microtransport induced by ultrasonic Lamb waves. *Appl Phys Lett* 1991;59(7):774–776. <https://doi.org/10.1063/1.105339>.
- <sup>44</sup>Rezk, AR, Ramesan, S, Yeo, LY. Plug-and-actuate on demand: Multimodal individual addressability of microarray plates using modular hybrid acoustic wave technology. *Lab Chip* 2018;18(3):406–411. <https://doi.org/10.1039/c7lc01099k>.
- <sup>45</sup>Baudoin, M, Gerbedoen, JC, Riaud, A, Matar, OB, Smagin, N, Thomas, JL. Folding a localized acoustical vortex on a flat holographic transducer: Miniaturized selective acoustical tweezers. *Sci Adv* 2019;5(4):eaav1967. <https://doi.org/10.1126/sciadv.aav1967>.
- <sup>46</sup>Kuznetsova, I, Nedospasov, I, Smirnov, A, Anisimkin, V, Roshchupkin, D, Signore, M-A, Franciosi, L, Kondoh, J, Serebrov, M, Kashin, V, et al. The peculiarities of the acoustic waves of zero-order focusing in lithium niobate plate. *Sensors* 2021;21(12):4000. <https://doi.org/10.3390/s21124000>.
- <sup>47</sup>Farnell, GW, Adler, EL. *Phys Acoust* 1972;9:35. <https://doi.org/10.1016/b978-0-12-395670-5.50007-6>.
- <sup>48</sup>Laidoudi, F, Boubenider, F, Caliendo, C, Hamidullah, M. Numerical investigation of Rayleigh, Sezawa and Love modes in C-axis tilted ZnO/Si for gas and liquid multimode sensor. *J Mech* 2020;36(1):7–18. <https://doi.org/10.1017/jmech.2019.14>.
- <sup>49</sup>Fu, YQ, Luo, JK, Nguyen, NT, Walton, AJ, Flewitt, AJ, Zu, XT, Li, Y, McHale, G, Matthews, A, Iborra, E, et al. Advances in piezoelectric thin films for acoustic biosensors, acoustofluidics and lab-on-chip applications. *Prog Mater Sci* 2017;89:31–91. <https://doi.org/10.1016/j.pmatsci.2017.04.006>.
- <sup>50</sup>Guo, YJ, Lv, HB, Li, YF, He, XL, Zhou, J, Luo, JK, Zu, XT, Walton, AJ, Fu, YQ. High frequency microfluidic performance of LiNbO<sub>3</sub> and ZnO surface acoustic wave devices. *J Appl Phys* 2014;116(2):024501. <https://doi.org/10.1063/1.4885038>.
- <sup>51</sup>Du, XY, Fu, YQ, Tan, SC, Luo, JK, Flewitt, AJ, Milne, WI, Lee, DS, Park, NM, Park, J, Choi, YJ, et al. ZnO film thickness effect on surface acoustic wave modes and acoustic streaming. *Appl Phys Lett* 2008;93(9):094105. <https://doi.org/10.1063/1.2970960>.
- <sup>52</sup>Jangj, M, Luo, JT, Tao, R, Reboud, J, Wilson, R, Cooper, JM, Gibson, D, Fu, YQ. Concentrated vertical jetting mechanism for isotropically focused ZnO/Si surface acoustic waves. *Int J Multiphase Flow* 2019;114:1–8. <https://doi.org/10.1016/j.ijmultiphaseflow.2019.02.002>.
- <sup>53</sup>Zhou, J, Tao, X, Luo, J, Li, Y, Jin, H, Dong, S, Luo, J, Duan, H, Fu, Y. Nebulization using ZnO/Si surface acoustic wave devices with focused interdigitated transducers. *Surf Coat Technol* 2019;367:127–134. <https://doi.org/10.1016/j.surfcoat.2019.03.078>.
- <sup>54</sup>Li, J, Biroun, MH, Tao, R, Wang, Y, Torun, H, Xu, N, Rahmati, M, Li, Y, Gibson, D, Fu, C, et al. Wide range of droplet jetting angles by thin-film based surface acoustic waves. *J Phys D Appl Phys* 2020;53(35):355402. <https://doi.org/10.1088/1361-6463/ab8f50>.
- <sup>55</sup>Gizelli, E, Stevenson, AC, Goddard, NJ, Lowe, CR. Surface skimming bulk waves: A novel approach to acoustic biosensors. *TRANSDUCERS'91: 1991 International Conference on Solid-State Sensors and Actuators. Digest of Technical Papers*. IEEE. 1991. pp.690–692.
- <sup>56</sup>Wixforth, A. Controlled agitation during hybridization. In *Microarrays in clinical diagnostics*. Springer. 2005. pp. 121–145.
- <sup>57</sup>Hough Love, AE. XI Chapter. Theory of the propagation of seismic waves. Some problems of geodynamics. Cornell University Library. 1911. pp. 144–178.
- <sup>58</sup>Hough Love, AE. Some problems of geodynamics: Being an essay to which the Adams prize, in the University of Cambridge, was adjudged in 1911. CUP Archive. 1967.
- <sup>59</sup>Du, J, Harding, GL, Ogilvy, JA, Dencher, PR, Lake, M. A study of Love-wave acoustic sensors. *Sens Actuators A* 1996;56(3):211–219. [https://doi.org/10.1016/s0924-4247\(96\)01311-8](https://doi.org/10.1016/s0924-4247(96)01311-8).
- <sup>60</sup>Jakoby, B, Vellekoop, MJ. Viscosity sensing using a Love-wave device. *Sens Actuators A* 1998;68(1–3):275–281. [https://doi.org/10.1016/s0924-4247\(98\)00017-x](https://doi.org/10.1016/s0924-4247(98)00017-x).
- <sup>61</sup>Kittmann, A, Durdaut, P, Zabel, S, Reermann, J, Schmalz, J, Spetzler, B, Meynert, D, Sun, NX, McCord, J, Gerken, M, et al. Wide band low noise Love wave magnetic field sensor system. *Sci Rep* 2018;8(1):278. <https://doi.org/10.1038/s41598-017-18441-4>.
- <sup>62</sup>Bleustein, JL. A new surface wave in piezoelectric materials. *Appl Phys Lett* 1968;13(12):412–413. <https://doi.org/10.1063/1.1652495>.
- <sup>63</sup>Gulyaev, YV. Electroacoustic surface waves in solids. *Sov Phys JTEP* 1969;9:63.
- <sup>64</sup>Zhang, C, Caron, JJ, Vetelino, JF. The Bleustein–Gulyaev wave for liquid sensing applications. *Sens Actuators B* 2001;76(1–3):64–68. [https://doi.org/10.1016/s0925-4005\(01\)00569-x](https://doi.org/10.1016/s0925-4005(01)00569-x).
- <sup>65</sup>Yang, J, Wang, J. Dynamic anti-plane problems of piezoceramics and applications in ultrasonics—A review. *Acta Mech Solida Sin* 2008;21(3):207–220. <https://doi.org/10.1007/s10338-008-0824-3>.
- <sup>66</sup>Collins, DJ, O'Rorke, R, Devendran, C, Ma, Z, Han, J, Neild, A, Ai, Y. Self-aligned acoustofluidic particle focusing and patterning in microfluidic channels from channel-based acoustic waveguides. *Phys Rev Lett* 2018;120(7):074502. <https://doi.org/10.1103/PhysRevLett.120.074502>.
- <sup>67</sup>Raymond, SJ, Collins, DJ, O'Rorke, R, Tayebi, M, Ai, Y, Williams, J. A deep learning approach for designed diffraction-based acoustic patterning in microchannels. *Sci Rep* 2020;10(1):8745. <https://doi.org/10.1038/s41598-020-65453-8>.
- <sup>68</sup>O'Rorke, R, Collins, D, Ai, Y. A rapid and meshless analytical model of acoustofluidic pressure fields for waveguide design. *Biomicrofluidics* 2018;12(2):024104. <https://doi.org/10.1063/1.5021117>.
- <sup>69</sup>Riaud, A, Baudoin, M, Thomas, J-L, Matar, OB. Cyclones and attractive streaming generated by acoustical vortices. *Phys Rev E* 2014;90(1):013008. <https://doi.org/10.1103/physreve.90.013008>.
- <sup>70</sup>Vanneste, J, Bühler, O. Streaming by leaky surface acoustic waves. *Proc R Soc A* 2011;467(2130):1779–1800. <https://doi.org/10.1098/rspa.2010.0457>.
- <sup>71</sup>Bennes, J, Alzuaga, S, Cherioux, F, Ballandras, S, Vairac, P, Manceau, J-F, Bastien, F. Detection and high-precision positioning of liquid droplets using SAW systems. *IEEE Trans Ultrason Ferroelectr Freq Control* 2007;54(10):2146–2151. <https://doi.org/10.1109/tuffc.2007.510>.
- <sup>72</sup>Ng, JW, Collins, DJ, Devendran, C, Ai, Y, Neild, A. Flow-rate-insensitive deterministic particle sorting using a combination of travelling and standing surface acoustic waves. *Microfluid Nanofluid* 2016;20(11):151. <https://doi.org/10.1007/s10404-016-1814-2>.
- <sup>73</sup>Vinh, PC. Scholte-wave velocity formulae. *Wave Motion* 2013;50(2):180–190. <https://doi.org/10.1016/j.wavemoti.2012.08.006>.

- <sup>74</sup>Aubert, V, Wunenburger, R, Valier-Brasier, T, Rabaud, D, Kleman, J-P, Poulain, C. A simple acoustofluidic chip for microscale manipulation using evanescent Scholte waves. *Lab Chip* 2016;16(13):2532–2539. <https://doi.org/10.1039/c6lc00534a>.
- <sup>75</sup>Nasr, S, Duclos, J, Leduc, M. Scholte wave characterization and its decay for various materials. *J Acoust Soc Am* 1990;87(2):507–512. <https://doi.org/10.1121/1.398921>.
- <sup>76</sup>Tayebi, M, O'Rorke, R, Wong, HC, Low, HY, Han, J, Collins, DJ, Ai, Y. Sub-micron particle trapping: Massively multiplexed submicron particle patterning in acoustically driven oscillating nanocavities (small 17/2020). *Small* 2020;16(17):2070095. <https://doi.org/10.1002/smll.202070095>.
- <sup>77</sup>Doinikov, AA, Gerlt, MS, Dual, J. Acoustic radiation forces produced by sharp-edge structures in microfluidic systems. *Phys Rev Lett* 2020;124(15):154501. <https://doi.org/10.1103/physrevlett.124.154501>.
- <sup>78</sup>Leibacher, I, Hahn, P, Dual, J. Acoustophoretic cell and particle trapping on microfluidic sharp edges. *Microfluid Nanofluid* 2015;19(4):923–933. <https://doi.org/10.1007/s10404-015-1621-1>.
- <sup>79</sup>Zhang, G, Cui, W, Pang, W, Liu, S, Ning, S, Li, X, Reed, M. Programmable and parallel trapping of submicron/nanoscale particles using acoustic micro-pillar array chip. *Adv Mater Interfaces* 2021;8(24):2101334. <https://doi.org/10.1002/admi.202101334>.
- <sup>80</sup>Mei, J, Zhang, N, Friend, J. Fabrication of surface acoustic wave devices on lithium niobate. *J Visualized Exp* 2020;160:e61013. <https://doi.org/10.3791/61013>.
- <sup>81</sup>Zhang, N, Horesh, A, Floer, C, Friend, J. Unapodization: A method to produce laterally uniform surface acoustic waves for acoustofluidics. *J Micromech Microeng* 2021;31(10):104001. <https://doi.org/10.1088/1361-6439/ac1d2d>.
- <sup>82</sup>Zhang, N, Zuniga-Hertz, JP, Zhang, FY, Gopesh, T, Fannon, MJ, Wang, J, Wen, Y, Patel, HH, Friend, J. Microliter ultrafast centrifuge platform for size-based particle and cell separation and extraction using novel omnidirectional spiral surface acoustic waves. *Lab Chip* 2021;21(5):904–915. <https://doi.org/10.1039/d0lc01012j>.
- <sup>83</sup>Riaud, A, Baudoin, M, Matar, OB, Becerra, L, Thomas, J-L. Selective manipulation of microscopic particles with precursor swirling Rayleigh waves. *Phys Rev Appl* 2017;7(2):024007. <https://doi.org/10.1103/physrevapplied.7.024007>.
- <sup>84</sup>Riaud, A, Baudoin, M, Thomas, J-L, Bou Matar, O. SAW synthesis with IDTs array and the inverse filter: Toward a versatile SAW toolbox for microfluidics and biological applications. *IEEE Trans Ultrason Ferroelectr Freq Control* 2016;63(10):1601–1607. <https://doi.org/10.1109/tuffc.2016.2558583>.
- <sup>85</sup>Hartmann, C, Wright, P, Kansy, R, Garber, E. Ultrasonics Symposium. IEEE. 1982. pp. 40–45. <https://doi.org/10.1109/ULTSYM.1982.197784>.
- <sup>86</sup>Shui, Y, Lin, JM, Wu, H, Wang, N, Chen, H. Optimization of single-phase, unidirectional transducers using three fingers per period. *IEEE Trans Ultrason Ferroelectr Freq Control* 2002;49(12):1617–1621. <https://doi.org/10.1109/tuffc.2002.1159840>.
- <sup>87</sup>Tan, MK, Friend, JR, Yeo, LY. Interfacial jetting phenomena induced by focused surface vibrations. *Phys Rev Lett* 2009;103(2):024501. <https://doi.org/10.1103/PhysRevLett.103.024501>.
- <sup>88</sup>Peng, T, Fan, C, Zhou, M, Jiang, F, Drummer, D, Jiang, B. Rapid enrichment of submicron particles within a spinning droplet driven by a unidirectional acoustic transducer. *Anal Chem* 2021;93(39):13293–13301. <https://doi.org/10.1021/acs.analchem.1c02914>.
- <sup>89</sup>Kodama, T, Kawabata, H, Sato, H, Yasuhara, Y. Design of low-loss SAW filters employing distributed acoustic reflection transducers. *Electron Commun Jpn (Part II: Electron)* 1987;70(9):32–44. <https://doi.org/10.1002/ecjb.4420700904>.
- <sup>90</sup>Morgan, DP. Quasi-static analysis of floating-electrode unidirectional SAW transducers (FEUDT's). 1999 IEEE Ultrasonics Symposium. Proceedings. International Symposium (Cat. No. 99CH37027). IEEE. 1999. Vol. 1. pp. 107–111.
- <sup>91</sup>Wright, PV. The natural single-phase unidirectional transducer: A new low-loss SAW transducer. IEEE 1985 Ultrasonics Symposium. IEEE. 1985. pp. 58–63.
- <sup>92</sup>Li, F, Cai, F, Liu, Z, Meng, L, Qian, M, Wang, C, Cheng, Q, Qian, M, Liu, X, Wu, J, et al. Phononic-crystal-based acoustic sieve for tunable manipulations of particles by a highly localized radiation force. *Phys Rev Appl* 2014;1(5):051001. <https://doi.org/10.1103/physrevapplied.1.051001>.
- <sup>93</sup>Assouar, B, Liang, B, Wu, Y, Li, Y, Cheng, J-C, Jing, Y. Acoustic metasurfaces. *Nat Rev Mater* 2018;3(12):460–472. <https://doi.org/10.1038/s41578-018-0061-4>.
- <sup>94</sup>Fall, D, Duquennoy, M, Ouaftouh, M, Smagin, N, Piwakowski, B, Jenot, F. Generation of broadband surface acoustic waves using a dual temporal-spatial chirp method. *J Acoust Soc Am* 2017;142(1):EL108–EL112. <https://doi.org/10.1121/1.4994676>.
- <sup>95</sup>Ding, X, Lin, S-CS, Lapsley, MI, Li, S, Guo, X, Chan, CY, Chiang, I-K, Wang, L, McCoy, JP, Huang, TJ. Standing surface acoustic wave (SSAW) based multichannel cell sorting. *Lab Chip* 2012;12(21):4228–4231. <https://doi.org/10.1039/c2lc40751e>.
- <sup>96</sup>Xu, G, Huang, J, Zhang, Y, Xie, L, Ni, Z, Huang, C, Yao, G, Tu, J, Guo, X, Zhang, D. Fourier acoustical tweezers: Synthesizing arbitrary radiation force using nonmonochromatic waves on discrete-frequency basis. *Phys Rev Appl* 2021;15(4):044037. <https://doi.org/10.1103/physrevapplied.15.044037>.
- <sup>97</sup>Yang, S, Tian, Z, Wang, Z, Rufo, J, Li, P, Mai, J, Xia, J, Bachman, H, Huang, P-H, Wu, M, et al. Harmonic acoustics for dynamic and selective particle manipulation. *Nat Mater* 2022;21:540. <https://doi.org/10.1038/s41563-022-01210-8>.
- <sup>98</sup>Wang, Q, Riaud, A, Zhou, J, Gong, Z, Baudoin, M. Acoustic radiation force on small spheres due to transient acoustic fields. *Phys Rev Appl* 2021;15(4):044034. <https://doi.org/10.1103/physrevapplied.15.044034>.
- <sup>99</sup>Bourquin, Y, Syed, A, Reboud, J, Ranford-Cartwright, LC, Barrett, MP, Cooper, JM. Rare-cell enrichment by a rapid, label-free, ultrasonic isopycnic technique for medical diagnostics. *Angew Chem Int Ed* 2014;53(22):5587–5590. <https://doi.org/10.1002/anie.201310401>.
- <sup>100</sup>Mutafopoulos, K, Spink, P, Lofstrom, CD, Lu, PJ, Lu, H, Sharpe, JC, Franke, T, Weitz, DA. Traveling surface acoustic wave (TSAW) microfluidic fluorescence activated cell sorter ( $\mu$ FACS). *Lab Chip* 2019;19(14):2435–2443. <https://doi.org/10.1039/c9lc00163h>.
- <sup>101</sup>Schmid, L, Franke, T. SAW-controlled drop size for flow focusing. *Lab Chip* 2013;13(9):1691–1694. <https://doi.org/10.1039/c3lc41233d>.
- <sup>102</sup>Jung, JH, Destgeer, G, Ha, B, Park, J, Sung, HJ. On-demand droplet splitting using surface acoustic waves. *Lab Chip* 2016;16(17):3235–3243. <https://doi.org/10.1039/c6lc00648e>.
- <sup>103</sup>Kang, P, Tian, Z, Yang, S, Yu, W, Zhu, H, Bachman, H, Zhao, S, Zhang, P, Wang, Z, Zhong, R, et al. Acoustic tweezers based on circular, slanted-finger interdigital transducers for dynamic manipulation of micro-objects. *Lab Chip* 2020;20(5):987–994. <https://doi.org/10.1039/c9lc01124b>.
- <sup>104</sup>Tian, Z, Yang, S, Huang, PH, Wang, Z, Zhang, P, Gu, Y, Bachman, H, Chen, C, Wu, M, Xie, Y, et al. Wave number-spiral acoustic tweezers for dynamic and reconfigurable manipulation of particles and cells. *Sci Adv* 2019;5(5):eaau6062. <https://doi.org/10.1126/sciadv.aau6062>.
- <sup>105</sup>Kharusi, MS, Farnell, GW. On diffraction and focusing in anisotropic crystals. *Proc IEEE* 1972;60(8):945–956. <https://doi.org/10.1109/proc.1972.8819>.
- <sup>106</sup>Castro, JO, Ramesan, S, Rezk, AR, Yeo, LY. Continuous tuneable droplet ejection via pulsed surface acoustic wave jetting. *Soft Matter* 2018;14(28):5721–5727. <https://doi.org/10.1039/c7sm02534c>.
- <sup>107</sup>Connacher, W, Orosco, J, Friend, J. Droplet ejection at controlled angles via acoustofluidic jetting. *Phys Rev Lett* 2020;125(18):184504. <https://doi.org/10.1103/physrevlett.125.184504>.
- <sup>108</sup>Brenker, JC, Collins, DJ, Van Phan, H, Alan, T, Neild, A. On-chip droplet production regimes using surface acoustic waves. *Lab Chip* 2016;16(9):1675–1683. <https://doi.org/10.1039/c5lc01341k>.
- <sup>109</sup>Zhang, P, Wang, W, Fu, H, Rich, J, Su, X, Bachman, H, Xia, J, Zhang, J, Zhao, S, Zhou, J, et al. Deterministic droplet coding via acoustofluidics. *Lab Chip* 2020;20(23):4466–4473. <https://doi.org/10.1039/d0lc00538j>.
- <sup>110</sup>Sesen, M, Alan, T, Neild, A. Microfluidic on-demand droplet merging using surface acoustic waves. *Lab Chip* 2014;14(17):3325–3333. <https://doi.org/10.1039/c4lc00456f>.
- <sup>111</sup>Bhattacharjee, PK, McDonnell, AG, Prabhakar, R, Yeo, LY, Friend, J. Extensional flow of low-viscosity fluids in capillary bridges formed by pulsed surface acoustic wave jetting. *New J Phys* 2011;13(2):023005. <https://doi.org/10.1088/1367-2630/13/2/023005>.
- <sup>112</sup>Xia, Y, Huang, L-X, Chen, H, Li, J, Chen, K-K, Hu, H, Wang, F-B, Ding, Z, Guo, S-S. Acoustic droplet vitrification method for high-efficiency preservation of rare cells. *ACS Appl Mater Interfaces* 2021;13(11):12950–12959. <https://doi.org/10.1021/acsami.1c01452>.

- <sup>113</sup>Luong, T-D, Phan, V-N, Nguyen, N-T. High-throughput micromixers based on acoustic streaming induced by surface acoustic wave. *Microfluid Nanofluid* 2011;10(3):619–625. <https://doi.org/10.1007/s10404-010-0694-0>.
- <sup>114</sup>Park, J, Destgeer, G, Afzal, M, Sung, HJ. Acoustofluidic generation of droplets with tunable chemical concentrations. *Lab Chip* 2020;20(21):3922–3929. <https://doi.org/10.1039/d0lc00803f>.
- <sup>115</sup>Shilton, R, Tan, MK, Yeo, LY, Friend, JR. Particle concentration and mixing in microdrops driven by focused surface acoustic waves. *J Appl Phys* 2008;104(1):014910. <https://doi.org/10.1063/1.2951467>.
- <sup>116</sup>Ren, L, Chen, Y, Li, P, Mao, Z, Huang, P-H, Rufo, J, Guo, F, Wang, L, McCoy, JP, Levine, SJ, et al. A high-throughput acoustic cell sorter. *Lab Chip* 2015;15(19):3870–3879. <https://doi.org/10.1039/c5lc00706b>.
- <sup>117</sup>Lei, Y, Hu, H. SAW-driven droplet jetting technology in microfluidic: A review. *Biomicrofluidics* 2020;14(6):061505. <https://doi.org/10.1063/5.0014768>.
- <sup>118</sup>Song, S, Zhou, J, Marcianò, A, Riaud, A. Contactless generation and trapping of hydrodynamic knots in sessile droplets by acoustic screw dislocations. *Phys Fluids* 2022;34(6):064101. <https://doi.org/10.1063/5.0093025>.
- <sup>119</sup>Tian, Z, Wang, Z, Zhang, P, Naquin, TD, Mai, J, Wu, Y, Yang, S, Gu, Y, Bachman, H, Liang, Y, et al. Generating multifunctional acoustic tweezers in Petri dishes for contactless, precise manipulation of bioparticles. *Sci Adv* 2020;6(37):eabb0494. <https://doi.org/10.1126/sciadv.abb0494>.
- <sup>120</sup>Baudoin, M, Thomas, JL, Sahely, RA, Gerbedoen, JC, Gong, Z, Sivery, A, Matar, OB, Smagin, N, Favreau, P, Vlandas, A. Spatially selective manipulation of cells with single-beam acoustical tweezers. *Nat Commun* 2020;11(1):4244. <https://doi.org/10.1038/s41467-020-18000-y>.
- <sup>121</sup>Sankaranarayanan, SKRS, Bhethanabotla, VR. Numerical analysis of wave generation and propagation in a focused surface acoustic wave device for potential microfluidics applications. *IEEE Trans Ultrason Ferroelectr Freq Control* 2009;56(3):631–643. <https://doi.org/10.1109/tuffc.2009.1079>.
- <sup>122</sup>Riaud, A, Thomas, J-L, Baudoin, M, Matar, OB. Taming the degeneration of Bessel beams at an anisotropic-isotropic interface: Toward three-dimensional control of confined vortical waves. *Phys Rev E* 2015;92(6):063201. <https://doi.org/10.1103/physreve.92.063201>.
- <sup>123</sup>John, F. Plane waves and spherical means applied to partial differential equations. Courier Corporation. 2004.
- <sup>124</sup>Laude, V, Jerez-Hanckes, CF, Balandras, S. Surface Green's function of a piezoelectric half-space. *IEEE Trans Ultrason Ferroelectr Freq Control* 2006;53(2):420–428. <https://doi.org/10.1109/tuffc.2006.1593381>.
- <sup>125</sup>Wang, Z, Tang, T, Chen, S, Chen, B. Field analysis and calculation of interdigital transducers with arbitrary finger shapes. *J Phys D Appl Phys* 2006;39(22):4902. <https://doi.org/10.1088/0022-3727/39/22/024>.
- <sup>126</sup>Wu, T-T, Tang, H-T, Chen, Y-Y. Frequency response of a focused SAW device based on concentric wave surfaces: Simulation and experiment. *J Phys D Appl Phys* 2005;38(16):2986. <https://doi.org/10.1088/0022-3727/38/16/035>.
- <sup>127</sup>Itoh, Y, Honjo, K. Recent advances in measurement techniques for microwave active devices and circuits. *IEICE Trans Electron* 2004;87(5):657–664.
- <sup>128</sup>Kock, WE. *Phys Acous* 1973;10:314.
- <sup>129</sup>Weser, R, Schmidt, H. In situ surface acoustic wave field probing in microfluidic structures using optical transmission interferometry. *J Appl Phys* 2021;129(24):244503. <https://doi.org/10.1063/5.0055231>.
- <sup>130</sup>Wang, Y, Theobald, P, Tyrer, J, Lepper, P. The application of scanning vibrometer in mapping ultrasound fields. *J Phys Conf Ser* 2004;1:037. <https://doi.org/10.1088/1742-6596/1/1/037>.
- <sup>131</sup>Brillouin, L. Maxwell's demon cannot operate: Information and entropy. I. *J Appl Phys* 1951;22(3):334–337. <https://doi.org/10.1063/1.1699951>.
- <sup>132</sup>Kwaaitaal, Th. Contribution to the interferometric measurement of sub-angstrom vibrations. *Rev Sci Instrum* 1974;45(1):39–41. <https://doi.org/10.1063/1.1686444>.
- <sup>133</sup>Royer, D, Dieulesaint, E. Optical probing of the mechanical impulse response of a transducer. *Appl Phys Lett* 1986;49(17):1056–1058. <https://doi.org/10.1063/1.97473>.
- <sup>134</sup>Ing, RK, Monchalin, JP. Broadband optical detection of ultrasound by two-wave mixing in a photorefractive crystal. *Appl Phys Lett* 1991;59(25):3233–3235. <https://doi.org/10.1063/1.105742>.
- <sup>135</sup>Rembe, C, Boedecker, S, Dräbenstedt, A, Pudewills, F, Siegmund, G. Heterodyne laser-Doppler vibrometer with a slow-shear-mode Bragg cell for vibration measurements up to 1.2 GHz. *Proc SPIE* 2008;7098:70980A. <https://doi.org/10.1117/12.802930>.
- <sup>136</sup>Muller, PB, Rossi, M, Marin, AG, Barnkob, R, Augustsson, P, Laurell, T, Kaehler, CJ, Bruus, H. Ultrasound-induced acoustophoretic motion of microparticles in three dimensions. *Phys Rev E* 2013;88(2):023006. <https://doi.org/10.1103/physreve.88.023006>.
- <sup>137</sup>Riaud, A, Baudoin, M, Bou Matar, O, Thomas, J-L, Brunet, P. On the influence of viscosity and caustics on acoustic streaming in sessile droplets: An experimental and a numerical study with a cost-effective method. *J Fluid Mech* 2017;821:384–420. <https://doi.org/10.1017/jfm.2017.178>.
- <sup>138</sup>Barnkob, R, Rossi, M. General defocusing particle tracking: Fundamentals and uncertainty assessment. *Exp Fluids* 2020;61(4):110. <https://doi.org/10.1007/s00348-020-2937-5>.
- <sup>139</sup>Tan, MK, Friend, JR, Yeo, LY. Direct visualization of surface acoustic waves along substrates using smoke particles. *Appl Phys Lett* 2007;91(22):224101. <https://doi.org/10.1063/1.2814054>.
- <sup>140</sup>Ha, BH, Lee, KS, Destgeer, G, Park, J, Choung, JS, Jung, JH, Shin, JH, Sung, HJ. Acoustothermal heating of polydimethylsiloxane microfluidic system. *Sci Rep* 2015;5(1):11851. <https://doi.org/10.1038/srep11851>.
- <sup>141</sup>Melde, K, Qiu, T, Fischer, P. Fast spatial scanning of 3D ultrasound fields via thermography. *Appl Phys Lett* 2018;113(13):133503. <https://doi.org/10.1063/1.5046834>.
- <sup>142</sup>Cox, L, Melde, K, Croxford, A, Fischer, P, Drinkwater, BW. Acoustic hologram enhanced phased arrays for ultrasonic particle manipulation. *Phys Rev Appl* 2019;12(6):064055. <https://doi.org/10.1103/physrevapplied.12.064055>.
- <sup>143</sup>Grinenko, A, MacDonald, MP, Courtney, CRP, Wilcox, PD, Demore, CEM, Cochran, S, Drinkwater, BW. Tunable beam shaping with a phased array acoustooptic modulator. *Opt Express* 2015;23(1):26–32. <https://doi.org/10.1364/oe.23.000026>.
- <sup>144</sup>Crockett, A, Rueckner, W. Visualizing sound waves with schlieren optics. *Am J Phys* 2018;86(11):870–876. <https://doi.org/10.1119/1.5042245>.
- <sup>145</sup>Sauer, W, Streibl, M, Metzger, TH, Haubrich, AGC, Manus, S, Wixforth, A, Peisl, J, Mazuelas, A, Härtwig, J, Baruchel, J. X-ray imaging and diffraction from surface phonons on GaAs. *Appl Phys Lett* 1999;75(12):1709–1711. <https://doi.org/10.1063/1.124797>.
- <sup>146</sup>Thibault, P, Bernard, I, Marmottant, P. Phase contrast microscopy characterization of standing surface acoustic waves for microfluidic applications. *Acoustofluidics 2021;Virtual Conference. CBMS*. 2021.
- <sup>147</sup>Tanski, WJ, Wittels, ND. SEM observations of SAW resonator transverse modes. *Appl Phys Lett* 1979;34(9):537–539. <https://doi.org/10.1063/1.90878>.
- <sup>148</sup>Mikhailov, R, Wu, F, Wang, H, Clayton, A, Sun, C, Xie, Z, Liang, D, Dong, Y, Yuan, F, Moschou, D, et al. Development and characterisation of acoustofluidic devices using detachable electrodes made from PCB. *Lab Chip* 2020;20(10):1807–1814. <https://doi.org/10.1039/c9lc01192g>.
- <sup>149</sup>Sun, C, Mikhailov, R, Fu, Y, Wu, F, Wang, H, Yuan, X, Xie, Z, Liang, D, Wu, Z, Yang, X. Flexible printed circuit board as novel electrodes for acoustofluidic devices. *IEEE Trans Electron Devices* 2020;68(1):393–398. <https://doi.org/10.1109/TED.2020.3039760>.
- <sup>150</sup>Brüning, R, Mensel, K, Kunze, R, Schmidt, H. New electronic device for driving surface acoustic wave actuators. *Procedia Chem* 2009;1(1):1111–1114. <https://doi.org/10.1016/j.proche.2009.07.277>.
- <sup>151</sup>Winkler, A, Harazim, S, Collins, DJ, Brüning, R, Schmidt, H, Menzel, SB. Compact SAW aerosol generator. *Biomed Microdevices* 2017;19(1):9. <https://doi.org/10.1007/s10544-017-0152-9>.
- <sup>152</sup>Fushimi, T, Marzo, A, Drinkwater, BW, Hill, TL. Acoustophoretic volumetric displays using a fast-moving levitated particle. *Appl Phys Lett* 2019;115(6):064101. <https://doi.org/10.1063/1.5113467>.



**Shuren Song** received his Ph.D. degree from Fudan University in 2022. His research interest focuses on acoustic streaming in microdroplets and multiphase flow modeling.



**Qi Wang** is currently a student pursuing a Ph.D. degree in the State Key Laboratory of ASIC and System, School of Microelectronics, Fudan University. Her research interests are Rayleigh acoustic streaming and biomedical sensors.



**Jia Zhou** received her Ph.D. degree from Fudan University in 2004. She is currently a Professor in the State Key Laboratory of ASIC and System, School of Microelectronics, Fudan University. Her research interests are in nano/microfluidics and in MEMS/NEMS-based chemical, biochemical, and biomedical sensors.



**Antoine Riaud** received his Ph.D. degree from Lille University (France) in 2017. He is currently an Associate Professor at the School of Microelectronics and in the State Key Laboratory of ASIC and System at Fudan University. His research interests focus on the design of actuators for microfluidic systems, including acoustic tweezers and electrowetting devices.